Estimating Fundamental Dynamic Properties of Structures with Supplemental Dampers by Means of Generalized Single Degree of Freedom Systems

Estimating fundamental dynamic properties of structures with supplemental dampers by means of Generalized Single Degree of Freedom systems

The dynamic response of complex structures can be estimated by means of Generalized Single Degree of Freedom (G-SDOF) systems. The original concept of G-SDOF system is revisited using an alternative viewpoint based on the equilibrium of the three resultant dynamic forces associated to the stiffness, mass and damping components, and applied to frame structures equipped with viscous dampers. In particular, it is shown that a generic structure with supplemental dampers can be reduced into two different G-SDOF idealizations, based on the global translational or rotational equilibrium. The mechanical analogies of the two G-SDOF systems provide physical insight into the dynamic behaviour of structures with viscous dampers, since their energy dissipation capacities can be graphically assessed in terms of the resultant dynamic forces and corresponding lever arms. The approach is applied to shear-type structures with specific dampers configurations resulting in proportionally damped systems. Novel analytical estimations of their first circular frequencies and modal damping ratios are obtained, providing upper- and lower-bounds of the exact values. Limitations in the use of the approach for structures with different dampers configurations resulting in highly non-proportionally damped systems are also discussed.

Keywords: Viscous dampers, Generalized SDOF system, Dynamic properties, Classical damping, Non-classical damping.

Introduction

Fluid viscous dampers are hydraulic devices which can be inserted in civil structures, including buildings, bridges, and lifeline equipment to mitigate the seismic-induced effects upon the structural elements thanks to the dissipation of part of the kinetic energy transmitted by the earthquake to the structure [Shen *et al.,* 1996; Soong *et al.,* 1997; Constantinou *et al.,* 1998; Chopra, 2001; Taylor *et al.,* 2002; Christopoulos *et al.,* 2006]. By increasing the damping ratio up to about 30%-50% of the critical value, such devices may reduce the structure peak displacements by a factor of 2 ÷2.5 thus reducing overall stresses in the structural elements [Lee *et al.,* 2000]. In the last 20 years, fluid viscous dampers have been successfully applied worldwide to hundreds of building structures [Web source: www.taylordevices.com].

The first fundamental scientific contributions in the field were focused on the basic principles of structural design and seismic response of building structures equipped with viscous dampers [Constantinou *et al.,* 1983; Reinhorn *et al.,* 1995; Hahn *et al.,* 1992; Constantinou *et al.,* 1993; Gluck *et al.,* 1996; Fu *et al.*, 1998]. In particular, the results of the research work carried out at Buffalo University by Constantinou and co-workers actually constitutes the main body of knowledge (MCEER report [Ramirez *et al.,* 2000] and [Ramirez *et al.,* 2002]) of the American seismic codes [FEMA 1050; ASCE/SEI 7-16]. More recently, the research efforts on structures with added dampers moved mainly to the optimal dampers placement [Cheng *et al.,* 1988; Takewaki, 1997, 2000, 2007; Shukla *et al.,* 1999; Singh *et al.,* 2001, 2002; Lopez-Garcia*,* 2001, 2002; Martinez-Rodrigo *et al.,* 2003; Lavan *et al.,* 2005, 2006; Liu *et al.,* 2005; Levy *et al.,* 2006; Pollini *et al.,* 2016].

In the last decades, some of the authors investigated the dynamic behavior of structures equipped with viscous dampers by means of theoretical and numerical studies providing insights into the dynamic response of frame structures equipped with different

configurations of added viscous dampers [Trombetti *et al.,* 2004, 2006, 2007; Silvestri *et al.,* 2010; Palermo *et al.,* 2018]. In detail, the work by Trombetti and Silvestri [2004] analyzed the dynamic response of specific classically damped systems, namely Mass Proportional Damping (MPD) and Stiffness Proportional Damping (SPD) systems. The results indicate that, within the class of classically damped systems, the MPD system provides superior performances in terms of minimum top-storey response variance to a Gaussian band limited white noise input. Then, the work by Trombetti and Silvestri [2006] investigated the modal properties of uniform frames equipped with MPD and SPD systems through the solution of the eigen-problem associated to the two damped systems. The results indicate that, under the assumption of "equal total size" constraint (that is equal total damping coefficient), the first modal damping ratio of the MPD system is always larger than that of the corresponding SPD system. The practical implementation of SPD and MPD systems in civil building structures was also discussed in [Trombetti and Silvestri 2004 and 2007, Silvestri and Trombetti 2007]. In detail, it was shown that if the added viscous dampers are placed in order to connect two adjacent storeys and all storey damping coefficients are selected to be proportional to the corresponding lateral storey stiffness, then the damping matrix of the system is proportional to the stiffness matrix (SPD system). Similarly, if the added viscous dampers are placed to connect each floor to a fixed point (ground or infinitely-stiff lateral-resisting element) and all storey damping coefficients are selected to be proportional to the corresponding floor masses, then the damping matrix of the system is proportional to the mass matrix (MPD system).

The damping ratio of structures equipped with added dampers has been often estimated through the Generalized Single Degree Of Freedom (G-SDOF) system approach, introduced by Chopra [Chopra, 2001]. For instance, the approach has been

recently applied for the design of structures with different types of dampers including viscous, viscoelastic and yielding dampers [Hu et al. 2020, Xie et al. 2020, Zhang et al. 2018].

In the present study, the traditional approach is revised and formulated in an alternative way to estimate the fundamental dynamic properties of frame structures equipped with supplemental viscous dampers. The method is applied to classically damped systems (namely, MPD and SPD systems) and approximate analytical expressions of the fundamental circular frequencies and the first modal damping ratios are obtained assuming a linear deformed shape vector. The effectiveness of the analytical estimations, that turned out to provide upper- and lower-bounds of the exact values, is evaluated by means of snap-back numerical simulations. Finally, considerations on the limitations of the G-SDOF system approach when applied to structures with non-classical damping systems are provided.

The Generalized SDOF system approach for structures with supplemental dampers

In the present section, the Generalized Single Degree Of Freedom (G-SDOF) system approach introduced by Chopra in chapter 8 of his textbook [Chopra, 2001] is revised with the aim of obtaining estimations of the fundamental dynamic properties (period of vibration and damping ratio) of structures equipped with supplemental viscous dampers. The original formulation presented by Chopra [Chopra, 2001] is based on the selection of a shape vector and application of the principle of virtual displacements with the aim of obtaining the equation of motion in terms of a single parameter, or generalized coordinate, describing the motion of the system. The analysis provides exact results for a system made by rigid blocks so that it can deflect only in

one shape. On the other hand, it provides only approximated results for structures with distributed mass and flexibility since their dynamic behaviour results from the superposition of the contribution of several modes of vibration [Chopra, 2001]. Nevertheless, if the shape vector is selected to be a good approximation of the fundamental mode of vibration, the approach can be applied to determine the approximated fundamental dynamic properties of the structure.

In the present paper the G-SDOF system is formulated in an alternative way through the direct imposition of the global dynamic translational or rotational equilibrium of the forces associated to stiffness, mass and damping components (the alternative view point as briefly presented by Chopra in section 9.1.4 of his textbook [Chopra, 2001]) without the use of the principle of virtual displacements. As such, for the same structural system two different G-SDOF systems will be identified in the next sections: the first one based on the imposition of the global translational equilibrium, the other one based on the global rotational equilibrium.

The studied systems and the assumed shape function

A *N*-storey shear frame structure equipped with a generic distribution of linear viscous dampers is considered (Fig. 1). The lateral storey stiffness of the frame at the *i*-th storey is referred to as k_i, while the floor mass at the generic *i*-th storey is referred to as m_i. The height of the *i*-th storey above the ground is indicated as z_i. A linear elastic behaviour for the frame elements is assumed. A linear constitutive law of the type $f_d = c \cdot v$ (where f_d is the force provided by the damper, c is the damping coefficient and v is the relative velocity between the two damper ends) is assumed for the damping mechanism. The generic *j*-th damper is characterized by coefficient c_j.

It is here assumed that the structure lateral deflected shape is described by a shape vector $\mathbf{d}=f(\zeta)$ where $f(\zeta)$ is a discrete function of a single scalar parameter ζ. The assumed shape vector can be selected in order to approximate the fundamental mode shape. Under this assumption, the time variation of the lateral floor displacement vector $\mathbf{u}(t)$ can be expressed as follows:

$$\mathbf{u}(t) = \mathbf{d} \cdot \gamma(t) \tag{1}$$

where $\gamma(t)$ is a scalar time-dependent response variable (also referred to as generalized coordinate response). Hereafter, for sake of simplicity, $\gamma(t)$ will be simply indicated as γ.

For the case of a regular N-storey frame with nearly uniform along-the-height distribution of lateral storey stiffness and floor mass and constant inter-storey height, a linear shape vector $\mathbf{d}$ (whose components are $d_i = i \cdot \delta$, δ indicating the inter-storey drift and $i = 1,2, \ldots N$) may provide a good enough approximation of the first mode shape $\boldsymbol{\phi}_1$ for preliminary design purposes [Palermo *et al.,* 2017]. In this case, the parameter ζ can be identified in the inter-storey drift δ.

Global dynamic equilibrium equations

The equation of motion of the N-storey system under free vibration can be expressed in matrix form as follows:

$$\mathbf{m}\ddot{\mathbf{u}}(t) + \mathbf{c}\dot{\mathbf{u}}(t) + \mathbf{k}\mathbf{u}(t) = \mathbf{0} \tag{2}$$

where: **m, c, k** are the mass, damping and stiffness matrices, respectively.

Eq. 2 is a system of N coupled translational equilibrium equations in the unknown vector $\mathbf{u}(t) = \{u_1(t) \quad u_2(t) \quad \ldots \quad u_N(t)\}$. Thanks to the kinematic assumption (Eq. 1), Eq. 2 can be approximated by:

$$\mathbf{m}\mathbf{d}\ddot{\gamma} + \mathbf{c}\mathbf{d}\dot{\gamma} + \mathbf{k}\mathbf{d}\gamma = \mathbf{0} \tag{3}$$

$\dot{\gamma}$ and $\ddot{\gamma}$ are the first and second time derivatives of γ, respectively.

Eq. 3 is a vectorial differential equation in the single unknown variable $\gamma(t)$. Mathematically, this corresponds to look for an approximated solution along the "direction" **d** provided by the kinematic assumption. If vector **d** is coincident with any exact mode shape $\boldsymbol{\phi}_i$, all N differential equations are exactly satisfied by the solution providing the i-th modal response.

Based on D'Alembert's principle, the dynamic equilibrium may be formulated based on an alternative viewpoint [Chopra, 2001], considering the system as the combination of three pure components: (1) a stiffness component, producing elastic resisting forces, (2) a damping component, producing damping forces and (3) a mass component, producing inertia forces (Fig. 2). More in detail, the external forces acting on the mass component can be grouped in the N-component vector $\mathbf{f}_I = \mathbf{m}\mathbf{d}\ddot{\gamma}$ ($f_{I,i}$ indicates the inertia force at the i-th storey). The external forces acting on the damping component can be grouped in the N-component vector $\mathbf{f}_D = \mathbf{c}\mathbf{d}\dot{\gamma}$ ($f_{D,i}$ indicates the damping force at the i-th storey). The external forces acting on the stiffness component can be grouped in the N-component vector $\mathbf{f}_S = \mathbf{k}\mathbf{d}\gamma$ ($f_{S,i}$ indicates the elastic force at the i-th storey).

Since the structural system has been substituted by a system of applied forces, and provided that it is supposed to be in dynamic equilibrium, it follows that the corresponding system of forces should satisfy both the global translational and rotational equilibrium. Hence, it is important to define the application point of each force. The generic i-th force (either the inertia, the damping, or the elastic force) is applied at the physical height z_i of the i-th storey (with respect to the ground level). The resultant dynamic forces and their corresponding application points (lever arms) of the

three sub-systems of forces are defined as: $F_I = \sum_{i=1}^{N} f_{I,i}$, $F_S = \sum_{i=1}^{N} f_{S,i}$, $F_D = \sum_{i=1}^{N} f_{D,i}$ and:

$z_M = \frac{\sum_{i=1}^{N} f_{I,i} \cdot z_i}{F_I} = \frac{\mathbf{z}^T \mathbf{md}}{\mathbf{i}^T \mathbf{md}}$, $z_K = \frac{\sum_{i=1}^{N} f_{S,i} \cdot z_i}{F_S} = \frac{\mathbf{z}^T \mathbf{kd}}{\mathbf{i}^T \mathbf{kd}}$, $z_C = \frac{\sum_{i=1}^{N} f_{D,i} \cdot z_i}{F_D} = \frac{\mathbf{z}^T \mathbf{cd}}{\mathbf{i}^T \mathbf{cd}}$, respectively.

The whole system of external forces is globally in equilibrium if both the global resultant force and the global moment resultant are null:

$$\sum_{i=1}^{N} f_{I,i} + \sum_{i=1}^{N} f_{D,i} + \sum_{i=1}^{N} f_{S,i} = 0 \tag{4}$$

$$\sum_{i=1}^{N} f_{I,i} \cdot z_i + \sum_{i=1}^{N} f_{D,i} \cdot z_i + \sum_{i=1}^{N} f_{S,i} \cdot z_i = 0 \tag{5}$$

or, equivalently, in matrix form:

$$\left(\mathbf{i}^T \mathbf{md}\right) \ddot{\gamma}_T + \left(\mathbf{i}^T \mathbf{cd}\right) \dot{\gamma}_T + \left(\mathbf{i}^T \mathbf{kd}\right) \gamma_T = 0 \tag{6}$$

$$\left(\mathbf{z}^T \mathbf{md}\right) \ddot{\gamma}_R + \left(\mathbf{z}^T \mathbf{cd}\right) \dot{\gamma}_R + \left(\mathbf{z}^T \mathbf{kd}\right) \gamma_R = 0 \tag{7}$$

where **i** is the *N*-component unitary vector and **z** is the *N*-component vector containing the heights of the application points.

Eqs. 6 and 7 are two scalar differential equations in the unknown variables $\gamma_T(t)$ and $\gamma_R(t)$, respectively. In other words, they represent the equations of motion of two single-degree-of-freedom systems. Hereafter they will be referred to as "Generalized Translational Oscillator" (GTO) with natural circular frequency ω_T and damping ratio ξ_T, and "Generalized Rotational Oscillator" (GRO), with natural circular frequency ω_R and damping ratio ξ_R.

The expressions of the generalized mass (M_T), damping coefficient (C_T) and stiffness (K_T) of the GTO are here reported:

$$M_T = \mathbf{i}^T \mathbf{md} \;;\; C_T = \mathbf{i}^T \mathbf{cd} \;;\; K_T = \mathbf{i}^T \mathbf{kd} \tag{8}$$

Similarly, the generalized mass (M_R), damping coefficient (C_R) and stiffness (K_R) of the GRO result to be:

$$M_R = \mathbf{z}^{\mathrm{T}}\mathbf{m}\mathbf{d};\ C_R = \mathbf{z}^{\mathrm{T}}\mathbf{c}\mathbf{d};\ K_R = \mathbf{z}^{\mathrm{T}}\mathbf{k}\mathbf{d} \tag{9}$$

Eqs. 6 and 7 can be rewritten making use of Eqs. 8-9 as follows:

$$M_T\ddot{\gamma}_T + C_T\dot{\gamma}_T + K_T\gamma_T = 0 \tag{10}$$

$$M_R\ddot{\gamma}_R + C_R\dot{\gamma}_R + K_R\gamma_R = 0 \tag{11}$$

It is interesting to notice that the mass ratio $\frac{M_R}{M_T}$, stiffness ratio $\frac{K_R}{K_T}$ and damping coefficient ratio $\frac{C_R}{C_T}$ are coincident to z_M, z_C and z_K respectively:

$$z_M = \frac{\mathbf{z}^T\mathbf{m}\mathbf{d}}{\mathbf{i}^T\mathbf{m}\mathbf{d}} = \frac{M_R}{M_T};\ z_C = \frac{\mathbf{z}^T\mathbf{c}\mathbf{d}}{\mathbf{i}^T\mathbf{c}\mathbf{d}} = \frac{C_R}{C_T};\ z_K = \frac{\mathbf{z}^T\mathbf{k}\mathbf{d}}{\mathbf{i}^T\mathbf{k}\mathbf{d}} = \frac{K_R}{K_T} \tag{12}$$

Note that the original procedure illustrated by [Chopra, 2001], based on the application of the principle of virtual displacements, leads to the following expressions of the generalized mass, stiffness and damping ratios:

$$\widetilde{M} = \mathbf{d}^{\mathrm{T}}\mathbf{m}\mathbf{d};\ \widetilde{C} = \mathbf{d}^{\mathrm{T}}\mathbf{c}\mathbf{d};\ \widetilde{K} = \mathbf{d}^{\mathrm{T}}\mathbf{k}\mathbf{d} \tag{13}$$

If $\mathbf{d}$ is coincident to a generic mode shape $\boldsymbol{\phi}_i$, then, in the undamped case, $F_I = F_S$ and $z_M \equiv z_K$, since both the global translational and rotational equilibrium equations are simultaneously satisfied. Also, when the assumed shape vector $\mathbf{d}$ is coincident with a structure mode shape $\boldsymbol{\phi}_i$, the expressions of the generalized properties of Eq. 13 become coincident with those of the modal properties.

Natural frequencies of the Generalized Oscillators

In the undamped case, Eqs. 6 and 7 reduce to:

$$\left(\mathbf{i}^T\mathbf{m}\mathbf{d}\right)\ddot{\gamma}_T + \left(\mathbf{i}^T\mathbf{k}\mathbf{d}\right)\gamma_T = 0 \tag{14}$$

$$\left(\mathbf{z}^T\mathbf{md}\right)\ddot{\gamma}_R + \left(\mathbf{z}^T\mathbf{kd}\right)\gamma_R = 0 \tag{15}$$

Eqs. 14 and 15 describe the motion of two SDOF systems of circular frequencies equal to:

$$\omega_T^2 = \frac{\mathbf{i}^T\mathbf{kd}}{\mathbf{i}^T\mathbf{md}} = \frac{K_T}{M_T} \tag{16}$$

$$\omega_R^2 = \frac{\mathbf{z}^T\mathbf{kd}}{\mathbf{z}^T\mathbf{md}} = \frac{K_R}{M_R} \tag{17}$$

By combining Eq. 12 with Eqs. 16 and 17 it is possible to relate the expressions of ω_T^2 and ω_R^2 to the arm ratio $\frac{z_K}{z_M}$:

$$\omega_R^2 = \omega_T^2 \cdot \frac{z_K}{z_M} \tag{18}$$

It follows that $\omega_R^2 \geq \omega_T^2$ when $z_K \geq z_M$.

The circular frequency of the G-SDOF system may be interpreted as a Rayleigh's quotient [Chopra 2001]:

$$\tilde{\omega}^2 = \frac{\mathbf{d}^T\mathbf{kd}}{\mathbf{d}^T\mathbf{md}} = \frac{\tilde{K}}{\tilde{M}} \tag{19}$$

The Rayleigh's quotient has the following property: it is always larger or equal than ω_1^2, namely $\tilde{\omega}^2 \geq \omega_1^2$.

When **d** is coincident to a system mode shape $\boldsymbol{\phi}_i$, then the three frequencies ω_T, ω_R and $\tilde{\omega}$ are all coincident with the *i*-th frequency of the system ω_i. More in general, the condition $\omega_T \cong \omega_R$ (or $z_M \cong z_K$) indicates that **d** is a good approximation of a system mode shape.

Damping ratios of the Generalized Oscillators

In the damped case (Eqs. 6 and 7), the damping ratios of the two generalized SDOF systems may be obtained as follows:

$$\xi_T = \frac{\mathbf{i}^T \mathbf{cd}}{2 \cdot \mathbf{i}^T \mathbf{md} \cdot \omega_T} = \frac{C_T}{2 \cdot M_T \cdot \omega_T} \tag{20}$$

$$\xi_R = \frac{\mathbf{z}^T \mathbf{cd}}{2 \cdot \mathbf{z}^T \mathbf{md} \cdot \omega_R} = \frac{C_R}{2 \cdot M_R \cdot \omega_R} \tag{21}$$

By combining Eqs. 12 and 18 with Eqs. 20 and 21 it is possible to relate the expressions of ξ_T and ξ_R to the arms z_K, z_M and z_C:

$$\xi_R = \xi_T \cdot \frac{z_C}{\sqrt{z_M z_K}} \tag{22}$$

It follows that $\xi_R \geq \xi_T$ when $z_C \geq \sqrt{z_M z_K}$.

For classically damped systems (i.e. the damping matrix is proportional either to the mass matrix or to the stiffness matrix, or to a combination of them), when **d** is coincident to a system mode shape $\boldsymbol{\phi}_i$, the two damping ratios ξ_T and ξ_R are both coincident with the *i*-th damping ratio ξ_i of the system.

Mechanical analogies of the Generalized Oscillators and interpretation of the modal analysis

The two Generalized Oscillators (GTO and GRO) may be graphically represented with the mechanical analogies (mass-spring-damper systems) and free-body diagrams as displayed in Figs. 3a and b. The free-body diagrams evidence the resultant inertia force F_I, the resultant damping force F_D, and the resultant elastic force F_S, and the corresponding lever arms with respect to point *O*.

The mechanical analogy of the GTO (Fig. 3a) allows to interpret the degree of freedom γ_T as non-dimensional displacement and Eq. (6) as the translational equilibrium

equation of the system characterized by mass M_T, translational stiffness K_T and damping coefficient C_T. In Fig. 3a, the dynamic system is represented as a "rigid body" on a movable clamp whose motion is governed by the translational equilibrium of the three resultant dynamic forces related to the mass, stiffness and damping components.

The mechanical analogy of the GRO (Fig. 3b) allows to interpret γ_R as a non-dimensional rotation and Eq. 7 as the rotational equilibrium equation of the system characterized by mass $M_R = M_T z_M$ (providing an inertia force F_I applied at height z_M), stiffness $K_R = K_T z_K$ (providing an elastic force F_S applied at height z_K) and damping coefficient $C_R = C_T z_C$ (providing a damping force F_D applied at height z_C). In Fig. 3b, the system is represented as a "rigid body" that is pinned at the base, whose motion is governed by the rotational equilibrium of the moments of the three resultant dynamic forces related to the mass, stiffness and damping components.

Note that the translational equilibrium can be interpreted as a rotational equilibrium with respect to a point at an infinite distance (Fig. 3a). Moreover, when vectors **d** and **z** are replaced with a generic mode shape vector $\boldsymbol{\phi}_n$, Eq. 7 becomes coincident to the equation of motion of the n-th mode of vibration, within the context of the classical modal analysis. The mechanical analogy of the n-th mode of vibration of a classically damped system (damping matrix proportional to the mass or stiffness matrix) is represented in Fig. 3c. In this particular case, it results that $z_M \equiv z_K \equiv z_C$. In other words, the modal analysis can be physically interpreted as the rotational equilibrium equation of the three dynamic resultant forces depicted in Fig. 3c whose lever arms can be obtained by assuming $\mathbf{z} = \boldsymbol{\phi}_n$. Furthermore, for the n-th mode of vibration, the imposition of the rotational equilibrium becomes equivalent to the imposition of the translational equilibrium equation, since $z_M \equiv z_K \equiv z_C$. To sum up, the dynamic equilibrium of the three generalized SDOF idealizations (GTO, GRO and the n-th mode

of vibration of the system) can be interpreted as the rotational equilibrium of the three resultant dynamic forces having different sets of lever arms.

Analytical estimations for uniform "classically damped" shear buildings: comparing different supplemental dampers configurations

As noted in the previous section, for regular frame structures with nearly uniform mass and storey stiffness distributions, the assumption of a linear shape vector may lead to a good enough estimation of the fundamental dynamic properties. Furthermore, the assumption of linear shape vector allows to obtain analytical estimations of the fundamental dynamic properties, thus providing insights into the dynamic behavior of damped frame structures.

For this purpose, the G-SDOF approach is applied for the case of a uniform shear frame structure equipped with a particular configuration of supplemental viscous dampers so that they can be treated as classically damped systems. The reference shear-type frame has (i) equal lateral storey stiffness k at all storeys, (ii) equal mass m at all floors, (iii) a fixed inter-storey height h so that the generic i-th component of vector z is $z_i=i\cdot h$, (iv) a bay width is equal to b. A linear shape vector **d** is considered so that its i-th component is $d_i = i \cdot \delta$, with δ indicating the inter-storey drift.

The following three types of damping systems are considered (Fig. 4):

- Stiffness Proportional Damping (SPD) system: the damping matrix **C** is proportional to the stiffness matrix **K**. A SPD system can be physically realized by inserting diagonal dampers, with damping coefficient proportional to storey lateral stiffnesses, at all storeys, each one connecting two adjacent storeys.

- Mass Proportional Damping (MPD) system: the damping matrix **C** is proportional to the mass matrix **M**. A MPD system can be physically realized connecting each floor to an infinitely stiff core through horizontal viscous dampers, with damping coefficients proportional to floor masses.

Dynamic properties of the G-SDOF systems

The generalized SDOF idealizations of uniform MPD and SPD systems are represented in Figs. 5 and 6, respectively. Each figure provides: (a) the assumed lateral deformed shape vector and the dynamic forces acting on the generic floor, (b) the GTO idealization, (c) the GRO idealization, (d) the free-body diagram.

First, the MPD system is considered. The damping coefficient of each viscous damper is denoted as c_{MPD}. The inertia, elastic and damping forces are shown in Fig. 5a and, thanks to the kinematic assumption, can be expressed as follows:

$$\begin{aligned} f_{I,i} &= m \cdot \ddot{d}_i = m \cdot i \cdot \ddot{\delta} \\ f_{D,i} &= c_{MPD} \cdot \dot{d}_i = c_{MPD} \cdot i \cdot \dot{\delta} \\ f_{S,i} &= k \cdot \left(d_i - d_{i-1}\right) - k \cdot \left(d_{i+1} - d_i\right) = \begin{cases} 0 & \text{for } i=1,2,...,N\text{-}1 \\ k \cdot \delta & \text{for } i=N \end{cases} \end{aligned} \tag{23}$$

Substitution of Eq. 23 into Eqs. 4 and 5 leads to the following global translational and rotational equilibrium equations in the degree of freedom δ:

$$\left(m \cdot \sum_{i=1}^{N} i\right) \ddot{\delta} + \left(c_{MPD} \cdot \sum_{i=1}^{N} i\right) \dot{\delta} + \left(k\right) \cdot \delta = 0 \tag{24}$$

$$\left(m \cdot h \cdot \sum_{i=1}^{N} i^2\right) \ddot{\delta} + \left(c_{MPD} \cdot h \cdot \sum_{i=1}^{N} i^2\right) \dot{\delta} + \left(k \cdot N \cdot h\right) \delta = 0 \tag{25}$$

where in Eq. 24 $\delta(t)=\gamma_T(t)$ corresponds to the degree of freedom (displacement) of the GTO of Fig. 3a, while in Eq. 25 $\delta(t)=h\cdot\gamma_R(t)$ corresponds to the degree of freedom of the GRO (either displacement $\delta(t)$ or rotation $\gamma_R(t)$) of Fig. 3b. The expressions within the round brackets in Eqs. 24 and 25 represent the generalized mass, stiffness and damping coefficients of the GTO and GRO idealizations of the MPD system.

The SPD system is now considered (Fig. 6). The diagonal inter-storey viscous dampers are inclined of an angle θ with respect to the horizontal direction and have the same linear damping coefficient c_{SPD}. The inertia, elastic and damping forces are shown in Fig. 6a and, thanks to the kinematic assumption, can be expressed as follows:

$$\begin{aligned} f_{I,i} &= m\cdot\ddot{d}_i = m\cdot i\cdot\ddot{\delta} \\ f_{D,i} &= c_{SPD,h}\cdot\left(\dot{d}_i-\dot{d}_{i-1}\right)-c_{SPD,h}\cdot\left(\dot{d}_{i+1}-\dot{d}_i\right)=\begin{cases} 0 \text{ for } i=1,2,...,N\text{-}1 \\ c_{IS,h}\cdot\dot{\delta} \text{ for } i=N \end{cases} \\ f_{S,i} &= k\cdot\left(d_i-d_{i-1}\right)-k\cdot\left(d_{i+1}-d_i\right)=\begin{cases} 0 & \text{for } i=1,2,...,N\text{-}1 \\ k\cdot\delta & \text{for } i=N \end{cases} \end{aligned} \tag{26}$$

where $c_{SPD,h}=c_{SPD}\cdot\cos^2\theta$ is the horizontal component of the damping coefficient.

Substitution of Eq. 26 into Eqs. 4 and 5 leads to the following global translational and rotational equilibrium equations in the unique degree of freedom δ:

$$\left(m\cdot\sum_{i=1}^{N}i\right)\ddot{\delta}+c_{SPD,h}\dot{\delta}+(k)\cdot\delta=0 \tag{27}$$

$$\left(m\cdot h\cdot\sum_{i=1}^{N}i^2\right)\ddot{\delta}+\left(c_{SPD,h}\cdot N\cdot h\cdot\right)\dot{\delta}+(k\cdot N\cdot h)\delta=0 \tag{28}$$

The expressions within the round bracktets in Eqs. 27 and 28 represent the generalized mass, stiffness and damping coefficients of the GTO and GRO idealizations of the SPD system. As expected, the expressions of the generalized mass and stiffness of the SPD systems are coincident with those of the MPD systems (since they depend on the mass and stiffness matrices only).

For the sake of clearness, the analytical expressions of the dynamic properties of the GTO and GRO corresponding to the MPD and SPD are collected in Tables 1-2. It is worth noticing that, for each system, c_{tot} indicates the sum of the damping coefficient of the individual dampers (i.e. $c_{tot} = N \cdot c_{SPD,h}$ for the SPD system and $c_{tot} = N \cdot c_{MPD}$ for the MPD system), while m_{tot} indicates the sum of the floor masses ($m_{tot} = N \cdot m$).

Effectiveness of the analytical predictions based on a linear shape vector

It is known that the mode shapes of classically damped systems, such as the MPD and SPD, are not depending on the size of dampers since the damping matrix is proportional to the mass and/or stiffness matrices. In such a case, the frequencies and damping ratios can be obtained through classical modal analysis [Chopra, 2001]. It can be of interest to evaluate the relative errors in the prediction of the first frequency and first damping ratio given by the analytical formulas derived in the previous sections based on the assumed linear deformed shape (Tables 1-2), with respect to those obtained according to classical modal analysis (e.g. using the exact mode shape).

Fig. 7 displays the normalized trend (with respect to $\omega_0 = \sqrt{k/m}$) of the first frequency ω_1 along with the two estimations ω_R and ω_T, with respect to the total number of storeys *N*.

It is possible to notice that the exact value of the frequency is in between the two estimations $\omega_T < \omega_1 < \omega_R$. The finding $\omega_R > \omega_T$ is due to the relationship (Eq. 18) existing between the two frequencies ω_R and ω_T and the arms of the resultant elastic and inertia forces (z_K and z_M). Indeed, for the case of a uniform shear-type frame system it is verified that $z_K > z_M$, as clearly shown by Figs. 5 and 6. Moreover, since

both vectors **d** and **z** are linear (i.e. **d** is proportional to **z**), the expression of ω_R^2 (Eq. 17) turns out to be a Rayleigh's quotient (Eq. 19), thus justifying the finding $\omega_R > \omega_1$.

The *relative errors* are evaluated as *(pred-exact)/exact*, where *pred* indicates the analytical prediction of the first frequency or first damping ratio, while *exact* indicates the corresponding value given by modal analysis. Fig. 8 displays the trends of the relative error as a function of the total number of storeys for the first frequency and first damping ratio, respectively. It can be noted that the relative errors remain below 10% up to a total number of storeys equal to 10. Fig. 8a shows that ω_R is an upper bound estimate of the first frequency (positive error), while ω_T is a lower bound estimate (negative error), as already highlighted above. Fig. 8b shows that ξ_T^{MPD} and ξ_R^{SPD} are upper bound estimates of the corresponding first damping ratios, while ξ_R^{MPD} and ξ_T^{SPD} are lower bound estimates. This is an expected result directly related to the relationship between damping ratios and arms (Eq. 22). Indeed, as clearly shown by Figs. 5 and 6, for the SPD system it is verified that $z_C > \sqrt{z_M z_K}$ (since $z_C \equiv z_K > z_M$), while for the MPD system it is verified that $z_C < \sqrt{z_M z_K}$ (since $z_C \equiv z_M < z_K$).

Simulated snap-back tests

In this section, the effectiveness of the analytical expressions of the damping ratios derived for the SPD and MPD systems are evaluated by means of numerical simulations carried out using the Finite Element Method (FEM). For this purpose, two five-storey shear-type frame structures equipped with an SPD or an MPD damping system (Fig. 9) are analyzed using the SAP2000 v18 software [Web source: www.csiamerica.com/products/sap2000]. A uniform floor mass m=100 t is considered

at all storeys. The lateral storey stiffness k is set equal to $1.0 \cdot 10^5$ kN/m. The inter-storey height is constant and equal to $h=3\ m$, while the bay width is equal to $b=6m$. The values of the first ω_1 and second ω_2 circular frequencies and of the bare frame is equal to 9.00 rad/s and 26 rad/s, while the first frequencies of the two G-SDOF systems estimated according to Eqs. 16 and 17 are equal to ω_R=9.53 rad/s and ω_T=8.17 rad/s.

For each analyzed system, the total damping coefficient c_{tot} is computed for two different values of target viscous damping ratio ξ_v (10% and 20%) according to the analytical equations (for the GRO system and using the value of the first circular frequency ω_1 as obtained from the FE model) as reported in Table 1 for the MPD system and in Table 2 for the SPD system. In addition to the viscous damping, an inherent damping ratio ξ_h=1% is assigned to all modes.

The logarithmic decrement method [Chopra, 2001] is used to compute the damping ratios from the time-history responses in free vibration triggered by an initial deformed shape proportional to the first mode shape. The values of damping ratios obtained from the numerical simulations ($\xi_{SAP2000}$) are reported in Table 3 and compared with the analytical estimations ($\xi_{v,R}$ and $\xi_{v,T}$) together with the values of the first circular frequencies. It can be noted that the analytical expressions provide accurate estimations of first modal damping ratios (also considering the 1% inherent damping) for both systems.

Equivalent damping ratios under the "equal total size" constraint

Since the analytical expressions of the first modal damping ratio based on the linear deformed shape provide accurate estimations for the case of uniform frames, they can be analyzed to compare the relative effectiveness of the two considered systems (namely the SPD and the MPD system). For this aim the assumption of "equal total

size" constraint [Takewaki 1997; Trombetti *et al.,* 2006] is considered: $c_{tot} = N \cdot c_{SPD,h} = N \cdot c_{MPD}$. Fig. 10 displays the trends of the analytical expressions of the damping ratios under "equal total size" constraint as a function of the total number of storeys *N* normalized to a unit value of ξ_R^{MPD} (e.g. the estimation of the damping ratio for system MPD based on the GRO idealization). It can be noted that the estimations of the damping ratios for the MPD system based on the GTO idealization are slightly larger than ξ_R^{MPD} with a 20% increase for a 10-storey building. Such difference is due to the use of different approximated expressions of the first frequency, whose trends with the total number of storeys is shown in Fig. 7. The first modal damping ratio of the SPD system decreases as the total number of storeys increases, thus indicating a reduced effectiveness with respect to the MPD system. For instance, for a 5-storey system, the damping ratio reduce of more than 10 times. This result is in accordance with the analytical derivations carried out in [Trombetti *et al.,* 2006] and has been used for the development of the so-called "five-step" [Silvestri *et al.,* 2010] and "direct five-step" [Palermo *et al.,* 2018] design procedures.

Limitations for non-classically damped systems

Analytical estimations based on a linear shape vector

In this section, uniform shear-type frame structures (as those considered in the previous section) equipped with viscous dampers leading to non-classically damped systems are considered. The aim is to obtain analytical expressions of the first modal damping ratio according to the G-SDOF idealizations and assuming a linear deformed shape. The following specific damper placements are considered:

- Inter-Storey (IS) placement: a single diagonal viscous damper (with damping coefficient c_{IS}) is placed to connect two consecutive storeys so that the viscous damper works for the inter-storey velocity.
- Fixed Point (FP) placement: a single viscous damper (with damping coefficient c_{FP}) is placed to connect a specific floor to a fixed point so that each damper works for the absolute storey velocity.

In particular, the acronyms IS-i and FP-i indicate a system with a damper located between the *i*-th and the the (*i*-1)-th storeys or at the *i*-th storey, respectively. For illustrative purposes, Figs. 11 a and b provide the graphical representation of a IS-3 and a FP-3 system, respectively.

The analytical estimations of the damping ratios (summarized in Table 4) are obtained considering both the GTO and GRO idealizations. Since linear systems are considered, the analytical relationships derived for IS and FP systems could be linearly combined to treat a more generic combination of inter-storey and fixed point dampers. For comparison purposes, the expressions derived in the previous section for the SPD and MPD systems are also included in Table 4.

Note that the GTO idealization based on a linear deformed shape leads to null values of damping ratios for IS systems with dampers placed at all storeys excluding the first. This result is a direct consequence of the assumed linear deformed shape and of the presence of a single inter-storey damper placed above the first inter-storey. Indeed, under this assumptions, as shown in Fig. 12, the horizontal components of the damping forces (associated with a damping coefficient $c_{IS,h} = c_{IS} \cdot \cos^2 \theta$) acting at the second and third floor have same magnitude but opposite directions, thus providing a null resultant damping force ($F_D = \sum_{i=1}^{N} f_{D,i} = 0$). Moreover, IS and FP systems with dampers located at

the first-storey are characterized by the same expressions of damping ratio since in both systems the added damper works for the first floor velocity.

It is convenient to normalize the expressions of the equivalent damping ratios summarized in Table 4 dividing each expression by the quantity $\frac{c_{tot}}{2m_{tot}\omega_R}$ (for the estimations based on GRO idealization) or by $\frac{c_{tot}}{2m_{tot}\omega_T}$ (for the estimations based on GTO idealization). Fig. 13 displays the trends of the normalized damping ratios (according to both GTO and GRO idealization) as function of the total number of storeys N for specific IS ad FP systems, namely IS-1 and FP-1 and FP-N (FP-N indicates an FP system with damper located at the top storey, i.e. the N-th storey).

Limitations of the analytical estimations based on the linear shape vector

From the theory of complex damping, it is known that non-classically damped systems are characterized by complex frequencies and complex mode depending on the amount of damping [Song *et al.,* 2008; Cheng, 2017; Liang *et al.,* 1991]. Indeed, the damping ratios of non-classically damped systems are no longer proportional to the total amount of damping provided by the added dampers (e.g. the sum of the damping coefficients of each damper) since they are highly dependent on both dampers location and size [Tovar *et al.,* 2004; Bajric *et al.,* 2018].

In light of this, in the present section the limitations of the simplified analytical equations for the estimation of the first damping ratios of 5-storey structures based on a linear deformed shape (reported in Table 4) are highlighted. For the sake of conciseness, the attention is focused on three selected IS systems and three selected FP systems (Fig.

14). These systems have been selected in order to encompass the different cases of a damper placed at a lower, intermediate, or upper storey. All structures have the same value of constant floor mass m and lateral stiffness k of those analyzed in the previous section.

The influence of the damping coefficients on the frequencies and damping ratios is evaluated through a parametric analysis by monotonically increasing the damping coefficient of the added viscous damper. An equivalent damping ratio ξ_c is defined and assumed varying between 0.01 to 1.0 (with an increment of 0.01). For each system, the damping coefficient (either c_{IS} *or* c_{FP}) of the added viscous damper corresponding to ξ_c is computed by inverting the corresponding equation reported in Table 4. In this way, a one-to-one correspondence between the damping coefficient of the added viscous damper and the damping ratio ξ_c is established. Thus, for each damper placement, a total number of 100 damped systems is analyzed according to the complex damping theory. For each complex eigenvalue λ_k, the corresponding undamped circular frequency ($\omega_k = |\lambda_k| = \sqrt{\mathrm{Re}(\lambda_k)^2 + \mathrm{Im}(\lambda_k)^2}$) and damping ratio ($\xi_k = \frac{\mathrm{Re}(\lambda_k)}{\omega_k}$) are determined and correlated to ξ_c. It is known that, for an underdamped system, each complex mode is characterized by a pair of complex conjugates eigenvalues. Furthermore, the undamped circular frequency of a non-classically damped is no more independent from the damping ratio, as for the case of a classically damped system [Palermo and Silvestri 2020].

The results of this analysis are summarized in Figs. 15-20 showing the trends of the circular frequencies and damping ratios associated to the first (related to eigenvalues λ_1 and λ_2) and second (related to eigenvalues λ_3 and λ_4) complex modes as a function of

ξ_c. First of all, as expected, the dependence of the circular frequencies and damping ratios on both the damper locations and damper sizes (through ξ_c) is highly non-linear.

It is worth noticing that systems IS-1 and FP-1 are characterized by the same dynamic behavior since their dampers work with the same velocity (indeed the first floor velocity is equal to the first inter-storey velocity). In this case (Fig. 15), for small values of damping coefficients (e.g. small values of ξ_c) leading to underdamped modes, the damping ratios associated to both the first and the second complex modes tend to increase (almost linearly) as the damping coefficient increases. Moreover, at first approximation, the damping ratio associated to the first complex mode has a slope similar to the straight line ξ_c (black dotted line), while the damping ratio associated to the second complex mode has a peak value equal to 0.12 (occurring at $\xi_c = 0.04$). Then, for a ξ_c value of 0.08, one damping ratio (green curve λ_3) associated to the second complex mode suddenly reaches a unit value (the mode becomes overdamped and accordingly the corresponding frequency vanishes and has no more a physical meaning), while the other one (cyan curve λ_4) progressively decreases with increasing ξ_c values. The frequency associated to the second complex mode (equal to 26 rad/s in the undamped case) first registers a fast increase for values of ξ_c less than 0.08, then it remains almost constant around 31.6 rad/s.

The damping ratio (red curve λ_1 and blue curve λ_2) associated to the first complex mode follows the trend of that associated to the second complex mode. Indeed, for a ξ_c value of 0.13, the red curve suddenly jumps to the critical condition (unitary damping ratio), while for larger ξ_c values the blue curve tend to slowly decrease (damping ratios associated to λ_2 and λ_3 become coincident). The corresponding

frequency first increases with ξ_c from 9 rad/s (undamped case) up to around 10.7 rad/s (for ξ_c equal to 0.2), then it remains almost constant.

These results indicate that both first-storey damper placements are characterized by a quite limited effectiveness, since the damping ratios dominating the dynamic behavior (the first and second ones) are quite small within the entire range of ξ_c.

The behavior of the other IS systems (Figs. 16-17) are qualitatively similar to that of system IS-1, but with even more reduced effectiveness, as evidenced by the smaller peak values of the first two damping ratios.

As far as FP systems are concerned (Figs. 18-20), it is possible to notice again that both circular frequencies and damping ratios have strong non-linear dependency on both damper location and damper size.

The behavior of system FP-2 (Fig. 18) is qualitatively similar that of system FP-1 (Fig. 15): the damping ratio (red curve λ_1 coincident with blue curve λ_2) associated to the first complex mode first monotonically increases up to a value of 0.33 that is achieved for a ξ_c value equal to 0.26, then it slowly decreases up to a value of ξ_c equal to 0.31. At this ξ_c value, the red curve suddenly jumps to the critical condition, while the blue one continues to slightly decrease for lager values of ξ_c; the corresponding frequency exhibits a slight increase from 9 rad/s up to around 13 rad/s. On the other hand, the damping ratio (green curve λ_3 coincident with cyan curve λ_4) associated with the second complex mode increases faster (more than linearly) reaching the critical condition (unit value) for a ξ_c value of around 0.3 without a sudden jump. These results indicate that, for the FP-2 system, the second mode can be effectively damped up to its critical value, whilst the first mode can be damped up to a value 0.33. Nevertheless, for

increasing ξ_c values, the second damping ratio exhibits a sudden sharp decrease up to a very small value (0.03) that remains constant for increasing ξ_c values (cyan curve); the corresponding frequency also exhibits a sudden jump (at a ξ_c value equal to 0.28) from a value of around 25 rad/s up to a value of around 40 rad/s. Overall, the system FP-2 shows a superior effectiveness with respect to system FP-1, since, for the "optimal" ξ_c value equal to 0.26, the first damping ratio is maximized (around 0.3) and the second damping ratio is close to 1.

For system FP-3, the damping ratio (red curve λ_1 coincident with blue curve λ_2) associated to the first complex mode increases more than linearly achieving the critical value for a ξ_c values equal to 0.57, without exhibiting any sudden drop. On the contrary, the damping ratio (green curve λ_3 and cyan curve λ_4) associated to the second complex mode achieves a peak value around 0.3. After the critical condition is reached, the second damping ratio starts to gradually decrease up to 0.2. Such behavior indicates that this FP placement has a very large effectiveness, since, for the "optimal" ξ_c value equal to 0.57, the first damping ratio is maximized (equal to 1.0) and the second damping ratio is close to its peak value (around 0.3).

For system FP-5, the first damping ratio gradually increases within the considered domain of ξ_c value, reaching the critical value around ξ_c =1.0. The second damping ratio exhibits a slower increase with a peak value of around 0.2 that is reached at ξ_c =1.0. Both frequencies exhibit smaller variations with respect to the previous cases. These results suggest that, within the considered range of damping coefficients, the system behaves, from a qualitative point of view, similarly to a classically damped system, for which an increase of the coefficient of the added damper leads to increased damping ratios, without modifying the frequencies.

The results obtained according to the theory of complex damping clearly indicate that adding a single viscous damper may lead to very different effectiveness, depending on both selected position and size. More specifically, IS placement leads to quite limited dissipation, while FP placement can lead to very high dissipation. This is due to a strong non-linear relationship between the damping coefficient of the added damper and the resulting damping ratio.

In general, the analytical expressions deduced from the G-SDOF approach appear of very limited applicability for non-classically damped systems. They can be applied only for very small ξ_c values, except for those FP systems that behave similarly to classically damped systems. A comprehensive parametric study is therefore required to fully investigate the dynamics of non-classically damped IS and FP systems. Such analysis is beyond the scope of the present work.

Simulated snap-back tests

In this final section, numerical simulations are carried out on selected IS and FP systems with the purpose of estimating the decay of the displacement responses at different storeys (to determine damping ratios using the logarithmic decrement method) in free vibrations from an initial deformed shape proportional to the undamped first mode shape. Selected time-history responses of the normalized displacements (with respect to the peak displacement at the top storey) at the first, third and top storey for one IS system (IS-2) and one FP system (FP-5) are reported in Figs. 21 and 22. The values of the damping ratio corresponding to the displacement response at the *i*-th storey computed according to the logarithmic decrement method is denoted as $\xi_{storey,i}$.

Values of $\xi_{storey,i}$ are reported in Table 5 for three cases (IS-2, FP-3 and FP-5) together with the values of the first damping ratio ξ_1 (ξ_c) from complex damping theory.

Inspections of the graphs reported in Figs. 21 and 22 and data collected in Table 5 clearly show that, for some systems, the time-history responses at the different storeys may decay with slightly different values of equivalent damping ratios. For instance, system IS-2 evidences a faster decay of motion at storeys 3 and 4 (damping ratios of 7%) with respect to those at the other storeys. In general, values of $\xi_{storey,i}$ are in reasonable good agreement with those obtained from complex damping theory (reported in the last row of Table 5). It can be also noticed that for the smaller value of target damping ratio (ξ_c =10%) both FP and IS systems are effective in reducing the displacements. On the contrary, for the larger value of target damping ratio (ξ_c =30%) only the two FP systems maintain their effectiveness ($\xi_{storey,i}$ values are between 38% and 40% for system FP-3 and equal to 24% for system FP-5), since the IS system is not effective in dissipating energy ($\xi_{storey,i}$ values are between 3% to 7%). Again, these numerical results reflect the trends obtained from the results of complex damping theory.

Conclusions

In the present work, the fundamental dynamic properties of frame structures equipped with supplemental linear viscous dampers have been investigating by revisiting the approach based on the Generalized-Single Degree Of Freedom (G-SDOF) system according to alternative view-point based on global equilibrium considerations. The approach is grounded on an assumed shape vector that approximates the lateral

deformed shape of the system. Then, the equation of motion of the G-SDOF system is formulated by imposing the global translational equilibrium or, alternatively, the global rotational equilibrium, thus leading to two different G-SDOF systems, namely a Generalized Translational Oscillator (GTO) and a Generalized Rotational Oscillator (GRO). For shear-type frame structures equipped with added dampers leading to classically damped systems, if the shape vector is an approximation of the fundamental mode shape, the dynamic properties of the two G-SDOF provide upper and lower bounds estimations of the fundamental frequency of vibration and corresponding modal damping ratio. If the shape vector is coincident with the first mode shape, the two G-SDOF systems have the same dynamic properties, that are, therefore, coincident with the exact first frequency and first modal damping ratio. Interesting mechanical analogies have been proposed allowing to physically interpret and compare the GTO, the GRO and the Generalized SDOF system corresponding to the *n*-th mode of vibration for a classically damped system.

For the case of uniform shear-type frames equipped with a Mass Proportionally Damped (MPD) or a Stiffness Proportionally Damped (SPD) system, the selection of a linear shape vector leads to analytical estimations of the dynamic properties, providing insights into the dynamic behavior of the systems. The results indicate that the errors in the estimations of the first frequency and first modal damping ratio remain below 10% up to a 10-storey structure. The analytical estimations of the damping ratios also allow to directly compare the effectiveness of the damping systems. It is confirmed that, under "equal total size" constraint, the MPD system has the largest efficiency, which is independent from the total number of storeys. On the contrary, the effectiveness of the SPD systems decreases with increasing total number of stories. The analytical formulas may be used by professional engineers in the preliminary design phase for the first

sizing of the damping coefficients of the added viscous dampers or to compare the global effectiveness of different damping systems for feasibility evaluations.

Finally, selected non-classically damped systems (namely shear-type structures equipped with a single damper) have been analyzed with the purpose of verifying the applicability and limitations of the method based on a linear shape vector. The results evidence that the estimations based on the G-SDOF system and on a linear mode shape are, in general, not effective for this class of damping systems. This is due to the strong non-linear dependence of the first modal damping ratio on both the location and size of the added dampers. Indeed, for some configurations, the increase in the size of the added dampers may even lead to a reduction in the dissipated energy. In this regard, more systematic analyses are necessary to provide further insight into the dynamic behavior of such specific damping systems.

Acknowledgements

Financial supports of Department of Civil Protection (DPC-Reluis 2014–2018 Grant—Research line 6: ‘‘Seismic isolation and dissipation’’ and 2019-2022 Research line WP15 “Contribution to codes for isolated and dissipative structures) is gratefully acknowledged.

The authors gratefully acknowledge Prof. Tommaso Ruggeri, Mathematical Department, University of Bologna for the useful suggestions about *N*-dimensional vector spaces.

References

ASCE/Structural Engineering Institute [2016] *Minimum design loads for buildings and other structures - ASCE/SEI 7-16*, Reston, VA.

Bajrić, A., Høgsberg, J. [2018] "Identification of damping and complex modes in structural vibrations", *Journal of Sound and Vibration* **431**, 367-389.

Cheng, F.Y., Pantelides, C.P. [1988] *Optimal placement of actuators for structural control*, Technical report NCEER-88-0037. State University of New-York at Buffalo, 1988.

Cheng, F.Y. [2017] *Matrix analysis of structural dynamics: applications and earthquake engineering*, CRC Press.

Chopra, A.K. [2001] *Dynamics of Structures: Theory and Applications to Earthquake Engineering, 2nd Edition*, Prentice Hall, Upper Saddle River, New Jersey.

Christopoulos, C., Filiatrault, A. [2006] *Principles of Passive Supplemental Damping and Seismic Isolation*, IUSS Press, Pavia, Italy, 2006.

Constantinou, M.C., Tadjbakhsh, I.G. [1983] "Optimum design of a first story damping system", *Computers & Structures* **17** (2), 305-310.

Constantinou, M.C., Symans, M.D. [1993] "Seismic response of structures with supplemental damping", *The Structural Design of Tall Buildings* **2**, 77-92.

Constantinou, M.C., Soong, T.T., Dargush, G.F. [1998] *Passive Energy Dissipation Systems for Structural Design and Retrofit, Monograph No. 1*, Multidisciplinary Center for Earthquake Engineering Research, Buffalo, New York.

Fu, Y., Kasai, K. [1998] "Comparative study of frames using viscoelastic and viscous dampers", *ASCE Journal of Structural Engineering* **124** (5), 513-522.

Gluck, N., Reinhorn, A.M., Gluck, J., Levy, R. [1996] "Design of supplemental dampers for control for structures", *ASCE Journal of Structural Engineering* **122** (12), 1394-1399.

Hahn, G.D., Sathiavageeswaran, K.R. [1992] "Effects of added-damper distribution on the seismic response of buildings", *Computers & Structures* **43** (5), 941-950.

Hu, X., Zhang, R., Ren, X., Pan, C., Zhang, X., & Li, H. [2020] "Simplified design method for structure with viscous damper based on the specific damping distribution pattern", *Journal of Earthquake Engineering*, https://doi.org/10.1080/13632469.2020.1719239.

Lee, D., Taylor, D.P. [2000] "Viscous damper development and future trends", *The Structural Design of Tall and Special Buildings* **10**(5), 311-320.

Lopez-Garcia, D. [2001] "A simple method for the design of optimal damper configurations in MDOF structures", *Earthquake Spectra* **17**(3), 387-398.

Lopez-Garcia, D., Soong, T.T., "Efficiency of a simple approach to damper allocation in MDOF structures", *Journal of Structural Control* **9**(1), 19-30.

Lavan, O., Levy, R. [2005] "Optimal design of supplemental viscous dampers for irregular shear-frames in the presence of yielding", *Earthquake Engineering and Structural Dynamics* **34**(8), 889-907.

Lavan, O., Levy, R. [2006] "Optimal peripheral drift control of 3D irregular framed structures using supplemental viscous dampers", *Journal of Earthquake Engineering* **10** (6), 903-923.

Levy, R., Lavan, O. [2006] "Fully stressed design of passive controllers in framed structures for seismic loadings", *Structural and Multidisciplinary Optimization* **32**(6), 485-498.

Liang, Z., Lee, G.C. [1991] *Damping of Structures: Part 1-Theory of Complex Damping*, National Center for Earthquake Engineering Research.

Liu, W., Tong, M., Lee, G.C. [2005] "Optimization methodology for damper configuration based on building performance indices", *ASCE Journal of Structural Engineering* **131**(11), 1746-1756.

Martinez-Rodrigo, M., Romero, M.L. [2003] "An optimum retrofit strategy for moment resisting frames with nonlinear viscous dampers for seismic applications", *Engineering Structures* **25** (2), 913-925.

NEHRP recommended seismic provisions for new buildings and other structures [2015] (FEMA 1050). Building Seismic Safety Council of the National Institute of Building Sciences, Washington, D.C.

Palermo, M., Silvestri, S., Trombetti, T. [2017] "On the peak inter-storey drift and peak inter-storey velocity profiles for frame structures", *Soil Dynamics and Earthquake Engineering* **94**, 18-34.

Palermo, M., Silvestri, S., Landi, L., Gasparini, G., Trombetti, T. [2018] "A "direct five-step procedure" for the preliminary seismic design of buildings with added viscous dampers", *Engineering Structures* **173,** 933-950.

Palermo, M., Silvestri, S. [2020], "Damping reduction factors for adjacent buildings connected by fluid-viscous dampers", *Soil Dynamics and Earthquake Engineering*, under review.

Pollini, N., Lavan, O., Amir, O. [2016] "Towards realistic minimum-cost optimization of viscous fluid dampers for seismic retrofitting", *Bulletin of Earthquake Engineering* **14**(3), 971-998.

Ramirez, O.M., Constantinou, M.C., Kircher, C.A., Whittaker, A.S., Johnson *et al.* [2000] *Development and evaluation of simplified procedures for analysis and design of buildings with passive energy dissipation systems - Report No. MCEER-00-0010*, Multidisciplinary Center for Earthquake Engineering Research, State University of New York at Buffalo.

Ramirez, O.M., Constantinou, M.C., Whittaker, A.S., Kircher, C.A., Chrysostomou, C.Z. [2002] "Elastic and inelastic seismic response of buildings with damping systems", *Earthquake Spectra* **18**(3), 531–547.

Reinhorn, A.M., Li, C., Constantinou, M.C. [1995] *Experimental and Analytical Investigation of Seismic Retrofit of Structures with Supplemental Damping, Part I - Fluid Viscous Damping devices, Technical Report NCEER-95-0001*, 1995. National Center for Earthquake Engineering Research, State University of New York at Buffalo.

Shen, K.L., Soong, T.T. [1996] "Design of energy dissipation devices based on concept of damage control", *ASCE Journal of Structural Engineering* **122**(1), 76-82.

Shukla, A.K., Datta, T.D. [1999] "Optimal use of viscoelastic dampers in building frames for seismic force", *ASCE Journal of Structural Engineering* **125**(4), 401-409.

Silvestri, S., Gasparini, G., Trombetti, T. [2010] "A five-step procedure for the dimensioning of viscous dampers to be inserted in building structures", *Journal of Earthquake Engineering* **14**(3), 417-447.

Silvestri, S., Trombetti, T. [2007] "Physical and Numerical Approaches for the Optimal Insertion of Seismic Viscous Dampers in Shear-Type Structures", *Journal of Earthquake Engineering* **11**(5)**, 787 - 828**.

Singh, M.P., Moreschi, L.M. [2001] "Optimal seismic response control with dampers", *Earthquake Engineering and Structural Dynamics* **30**, 553-572.

Singh, M.P., Moreschi, L.M. [2002] "Optimal placement of dampers for passive response control", *Earthquake Engineering and Structural Dynamics* **31**, 955-976.

Song, J.W., Chu, Y.L., Liang, Z., Lee, G.C. [2008] *Modal analysis of generally damped linear structures subjected to seismic excitations - Technical Report MCEER-08-0005*, State University of New York at Buffalo.

Soong, T.T., Dargush, G.F. [1997] *Passive Energy Dissipation Systems in Structural Engineering*, John Wiley & Sons, Baffins Lane, Chichester, United Kingdom.

Takewaki, I. [1997] "Optimal damper placement for minimum transfer functions", *Earthquake Engineering and Structural Dynamics* **26**, 1113-1124.

Takewaki, I. [2000] "Optimal damper placement for critical excitation", *Probabilistic Engineering Mechanics* **15**, 317-325.

Takewaki, I. [2007] "Earthquake Input Energy to Two Buildings Connected by Viscous Dampers", *ASCE Journal of Structural Engineering* **133**(5), 620-628.

Taylor, D.P., Constantinou, M.C. [2002] *Fluid Dampers for Applications of Seismic Energy Dissipation and Seismic Isolation*, Technical Report 2002, Taylor Devices Inc., 90 Taylor Drive, North Tonawonda, NY.

Tovar, C., Lopez, O.A. [2004] "Effect of the position and number of dampers on the seismic response of frame structures", *Proc. Of the 2nd World Conference of Earthquake Engineering*, Vancouver, BC, Canada.

Trombetti, T., Silvestri, S. [2004] "Added viscous dampers in shear-type structures: the effectiveness of mass proportional damping", *Journal of Earthquake Engineering*, **8**(2), 275-313.

Trombetti, T., Silvestri, S. [2006] "On the modal damping ratios of shear-type structures equipped with Rayleigh damping systems", *Journal of Sound and Vibration* **292** (2), 21-58.

Trombetti, T., Silvestri, S. [2007] “Novel schemes for inserting seismic dampers in shear-type systems based upon the mass proportional component of the Rayleigh damping matrix”, *Journal of Sound and Vibration* **302** (3), 486-526.

Web source: www.csiamerica/products/sap2000

Web source: www.taylordevices.com.

Xie, L., Zhang, L., Pan, C., Zhang, R., Chen, T. [2020] “Uniform damping ratio-based design method for seismic retrofitting of elastoplastic RC structures using viscoelastic dampers”, *Soil Dynamics and Earthquake Engineering,* **128**, 105866.

Zhang, R.F., Wang, C., Pan, C., Shen, H., Ge, Q.Z., Zhang, L.Q. [2018] “Simplified design of elastoplastic structures with metallic yielding dampers based on the concept of uniform damping ratio”, *Engineering Structures* **176**, 734-745.

Table 1. Analytical expressions of the dynamic properties of MPD systems according to the GRO and GTO idealizations.

Generalized mass	**Generalized stiffness**	**Generalized damping coefficient**	**Circular frequency**	**Damping ratio**
$M_R = \frac{m \cdot h \cdot N \cdot (N+1)(2N+1)}{6}$	$K_R = k \cdot h \cdot N$	$C_R^{MPD} = \frac{c_{MPD} \cdot h \cdot N \cdot (N+1)(2N+1)}{6}$	$\omega_R = \omega_0 \sqrt{\frac{6}{(N+1)(2N+1)}}$	$\xi_R^{MPD} = \frac{c_{tot}}{2 \cdot m_{tot} \cdot \omega_R}$
$M_T = \frac{m \cdot N \cdot (N+1)}{2}$	$K_T = k$	$C_T^{MPD} = \frac{c_{MPD} \cdot N \cdot (N+1)}{2}$	$\omega_T = \omega_0 \sqrt{\frac{2}{N(N+1)}}$	$\xi_T^{MPD} = \frac{c_{tot}}{2 \cdot m_{tot} \cdot \omega_T}$

Table 2. Analytical expressions of the dynamic properties of SPD systems according to GRO and GTO idealizations.

Generalized mass	**Generalized stiffness**	**Generalized damping coefficient**	**Circular frequency**	**Damping ratio**
$M_R = \frac{m \cdot h \cdot N \cdot (N+1)(2N+1)}{6}$	$K_R = k \cdot h \cdot N$	$C_R^{SPD} = c_{SPD,h} \cdot h \cdot N$	$\omega_R = \omega_0 \sqrt{\frac{6}{(N+1)(2N+1)}}$	$\xi_R^{SPD} = \frac{c_{tot}}{2 m_{tot} \omega_R} \left(\frac{6}{(N+1)(2N+1)} \right)$
$M_T = \frac{m \cdot N \cdot (N+1)}{2}$	$K_T = k$	$C_T^{SPD} = c_{SPD,h}$	$\omega_T = \omega_0 \sqrt{\frac{2}{N(N+1)}}$	$\xi_T^{SPD} = \frac{c_{tot}}{2 m_{tot} \omega_T} \left(\frac{2}{N(N+1)} \right)$

Table 3. Damping ratios from numerical simulations through snap-back tests.

		MPD	**SPD**
ξ_v =10%	**c_{tot} [kN s/m]**	900	9905
	$\xi_{v,R}$	0.09	0.09
	$\xi_{v,T}$	0.11	0.08
	$\xi_{SAP2000}$	0.11	0.10
ξ_v =20%	**c_{tot} [kN s/m]**	1810	19811
	$\xi_{v,R}$	0.19	0.19
	$\xi_{v,T}$	0.22	0.16
	$\xi_{SAP2000}$	0.21	0.19

Table 4. Analytical expressions of the damping ratio of SPD, MPD, IS-i and FP-i systems according to GRO and GTO idealizations.

System type	GRO idealization	GTO idealization
SPD	$\xi_R^{SPD} = \frac{c_{tot}}{2m_{tot}\omega_R}\left(\frac{6}{(N+1)(2N+1)}\right)$	$\xi_T^{SPD} = \frac{c_{tot}}{2m_{tot}\omega_T}\left(\frac{2}{N(N+1)}\right)$
MPD	$\xi_R^{MPD} = \frac{c_{tot}}{2 \cdot m_{tot} \cdot \omega_R}$	$\xi_T^{MPD} = \frac{c_{tot}}{2 \cdot m_{tot} \cdot \omega_T}$
IS-i	$\xi_R^{IS,i} = \frac{c_{tot}}{2m_{tot}\omega_R}\left(\frac{6}{(N+1)(2N+1)}\right)$	$\xi_T^{IS,i} = 0$
IS-1	$\xi_R^{IS,1} = \frac{c_{tot}}{2m_{tot}\omega_R}\left(\frac{6}{(N+1)(2N+1)}\right)$	$\xi_T^{IS,1} = \frac{c_{tot}}{2m_{tot}\omega_T}\left(\frac{2}{N(N+1)}\right)$
FP-i	$\xi_R^{FP,i} = \frac{c_{tot}}{2m_{tot}\omega_R}\left(\frac{6i^2}{(N+1)(2N+1)}\right)$	$\xi_T^{FP,i} = \frac{c_{tot}}{2m_{tot}\omega_T}\left(\frac{2i}{N+1}\right)$
FP-1	$\xi_R^{FP,1} = \frac{c_{tot}}{2m_{tot}\omega_R}\left(\frac{6}{(N+1)(2N+1)}\right)$	$\xi_T^{FP,1} = \frac{c_{tot}}{2m_{tot}\omega_T}\left(\frac{2}{N+1}\right)$

Table 5. Comparison between the values of the storey damping ratios $\xi_{storey,i}$ as obtained from the numerical simulations and ξ_c and $\xi_1(\xi_c)$.

	IS-2		**FP-3**		**FP-5**	
	(ξ_c =10%)	**(ξ_c =30%)**	**(ξ_c =10%)**	**(ξ_c =30%)**	**(ξ_c =10%)**	**(ξ_c =30%)**
$\xi_{storey,1}$ **[%]**	5	3	12	38	8	24
$\xi_{storey,2}$ **[%]**	5	3	13	38	8	24
$\xi_{storey,3}$ **[%]**	7	7	13	39	8	24
$\xi_{storey,4}$ **[%]**	7	7	13	40	8	24
$\xi_{storey,5}$ **[%]**	6	6	13	40	8	24
ξ_1 **(ξ_c) [%]**	6	4	12	40	8	24

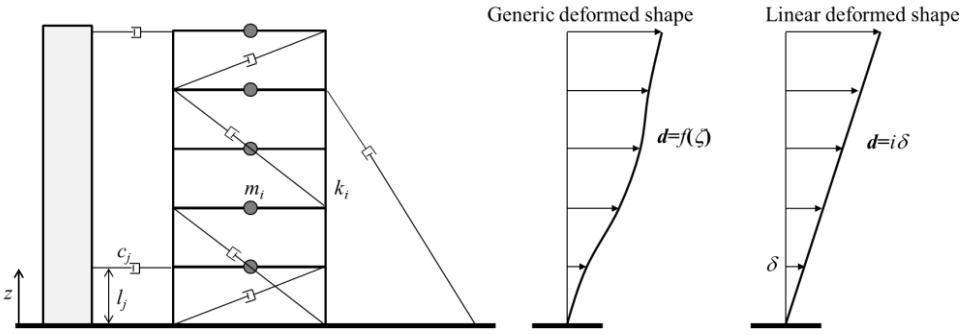

Figure 1. The N-storey frame structure equipped with a generic distribution of added viscous dampers.

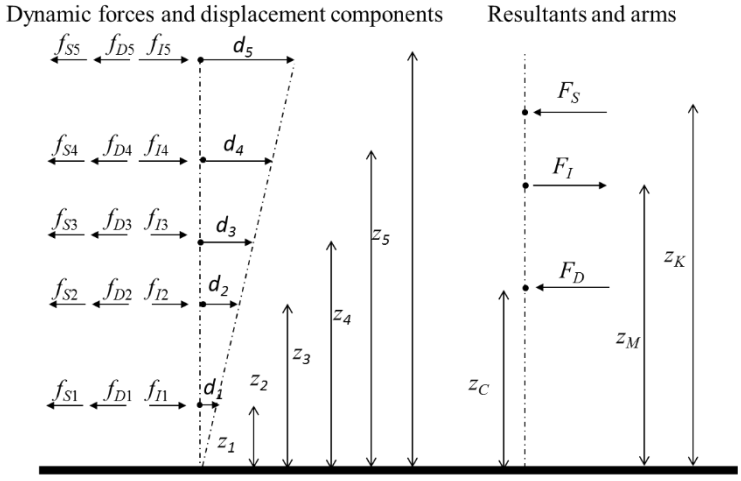

Figure 2. External dynamic forces and resultants.

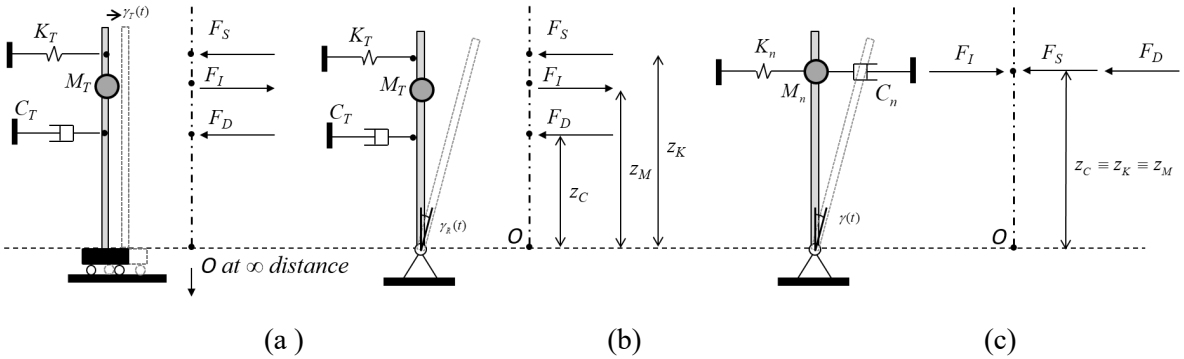

Figure 3. Mechanical analogy and free-body diagram: (a) GTO idealization; (b) GRO idealization; (c) Generalized SDOF system corresponding to the *n*-th mode of vibration for a classically damped system.

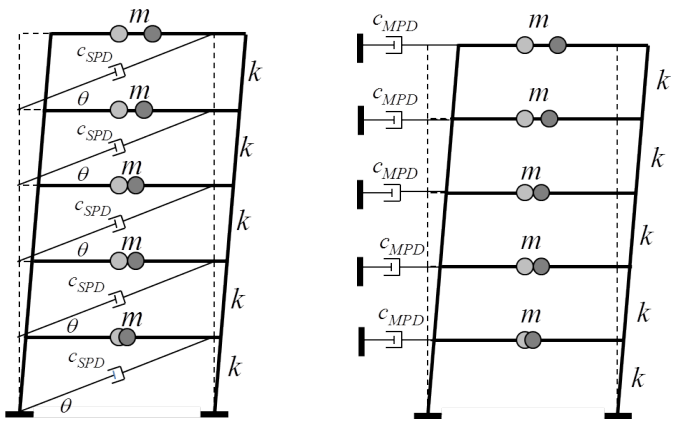

Figure 4. (a) SPD system. (b) MPD system.

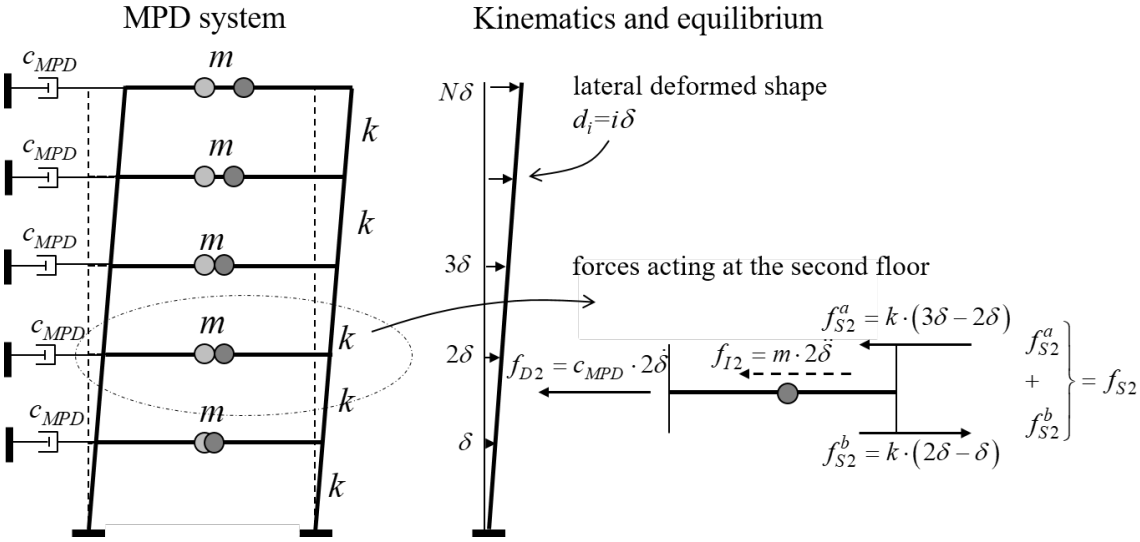

(a)

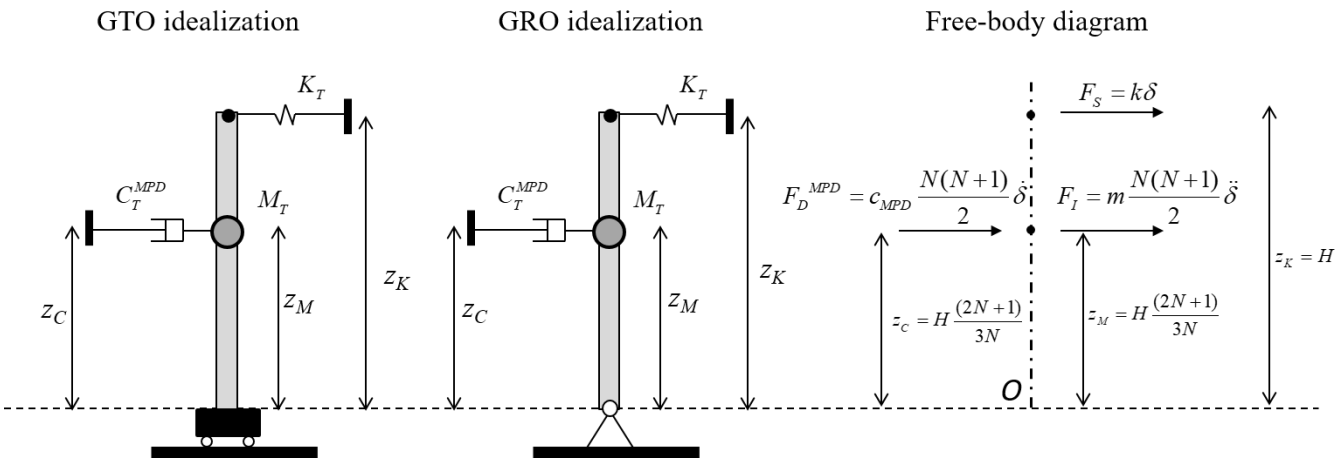

(b) (c) (d)

Figure 5. MPD system and its corresponding G-SDOF idealisations: (a) kinematics and equilibrium; (b) GTO idealization, (c) GRO idealization, (d) free-body diagram.

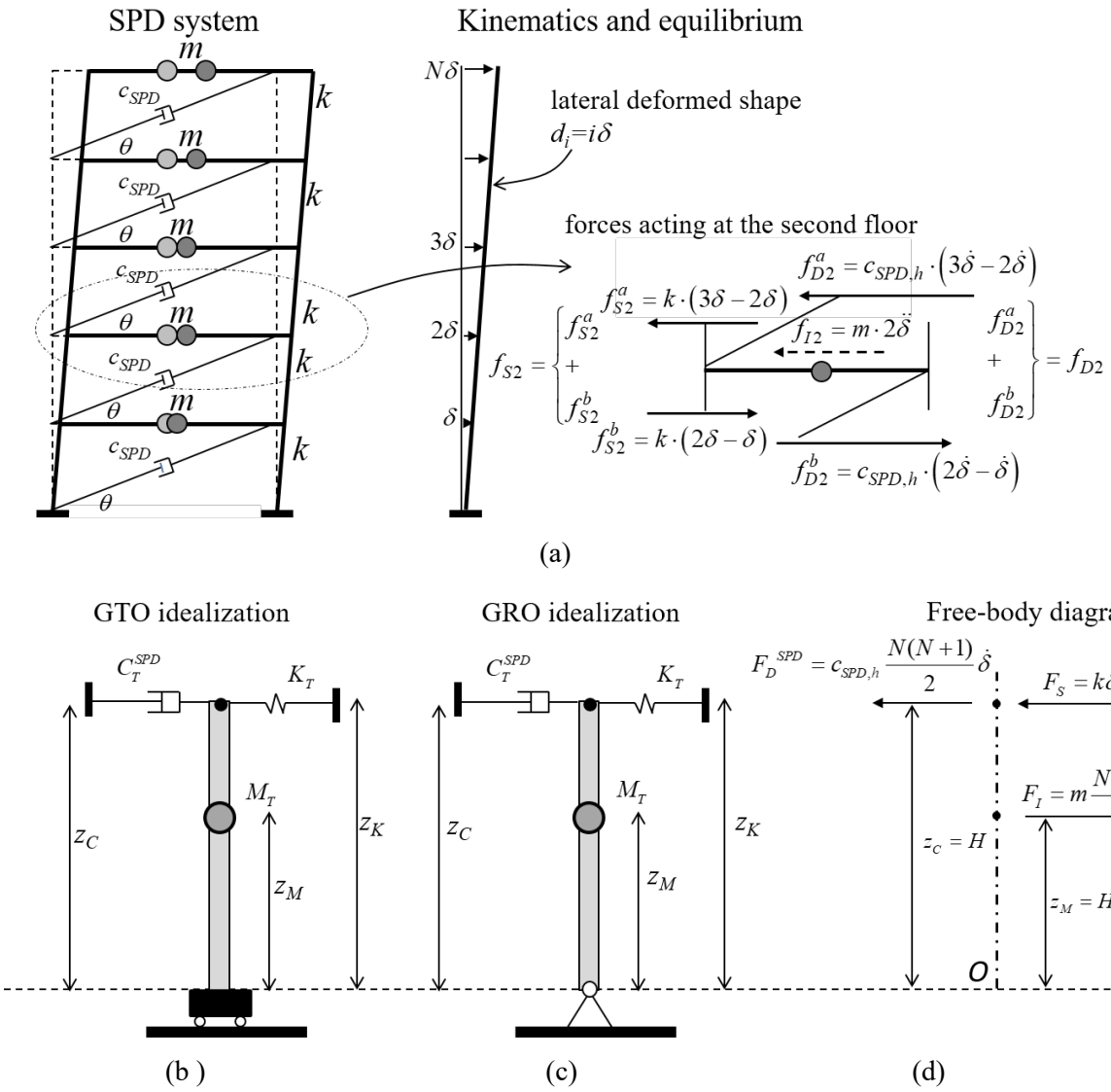

Figure 6. SPD system and its corresponding G-SDOF idealisations: (a) kinematics and equilibrium; (b) GTO idealization, (c) GRO idealization, (d) free-body diagram.

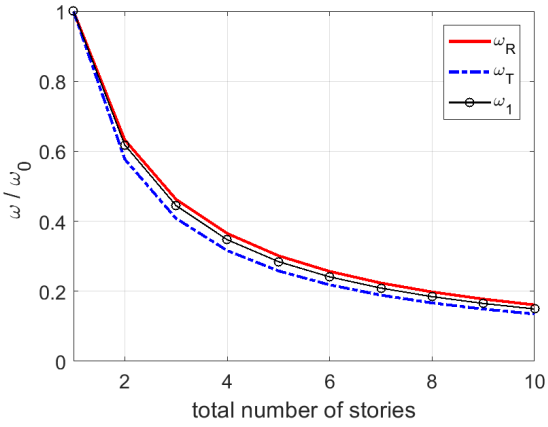

Figure 7. ω_1 / ω_0 vs total number of storeys.

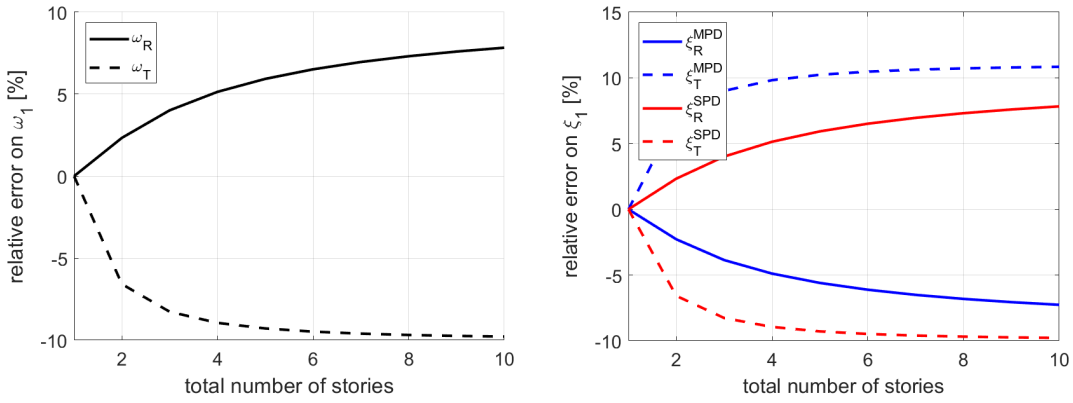

(a) (b)

Figure 8. Relative errors: (a) first frequencies; (b) first damping ratios.

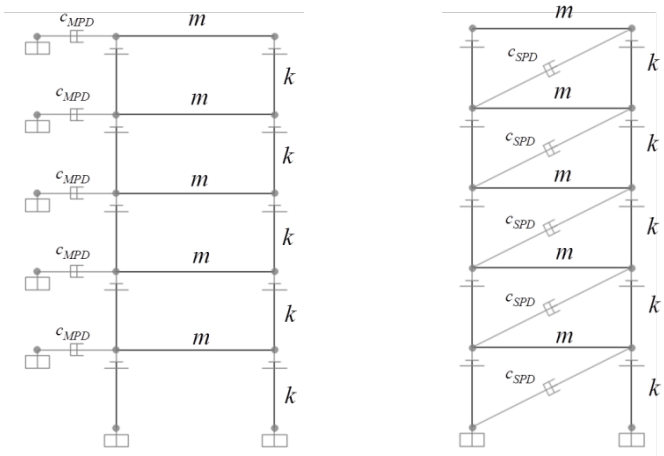

(a) (b)

Figure 9. The analyzed FE models: (a) MPD; (b) SPD.

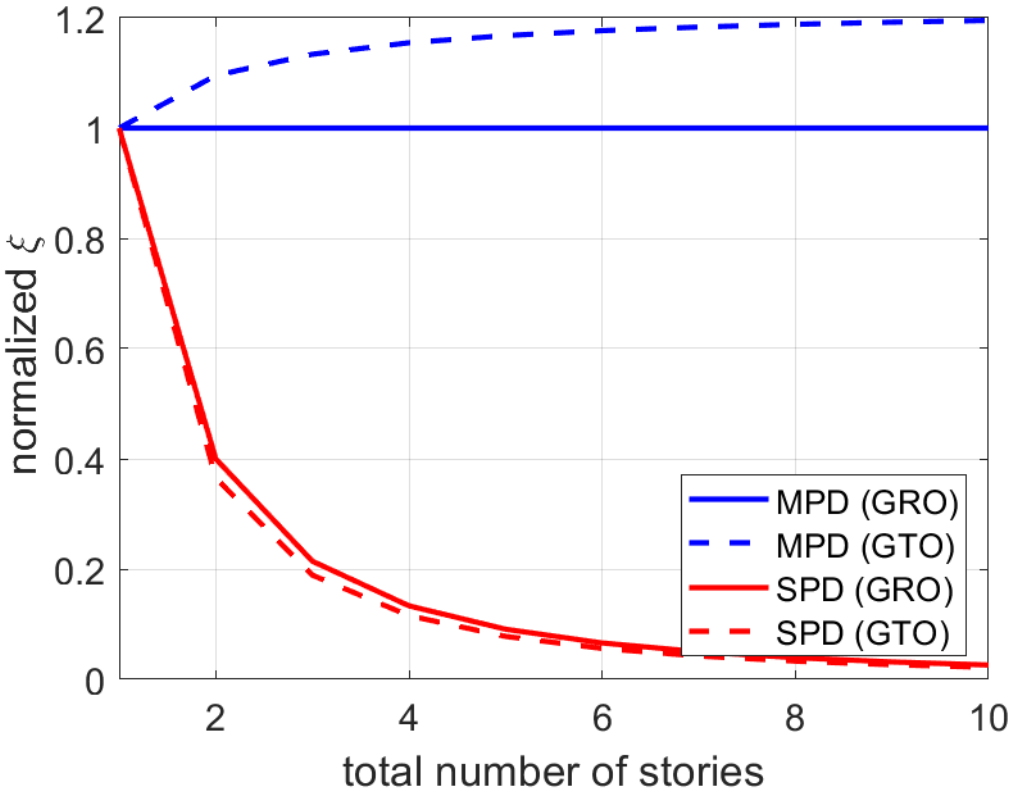

Figure 10. Normalized damping ratio under “equal total size” constraint.

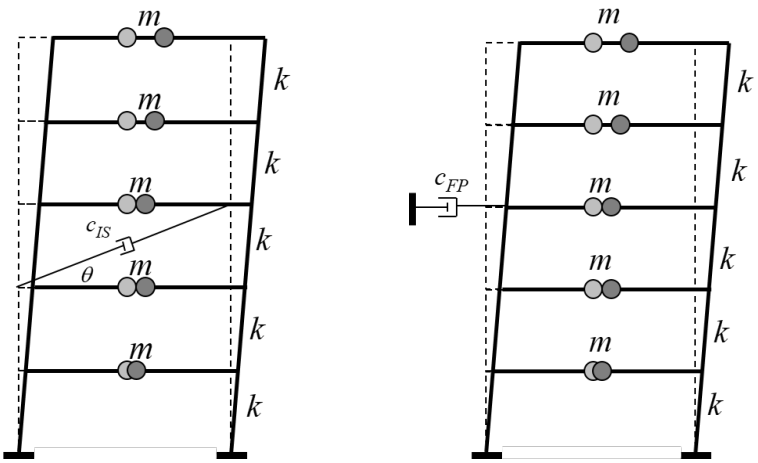

(a) (b)

Figure 11. (a) IS-3 system. (b) FP-3 system.

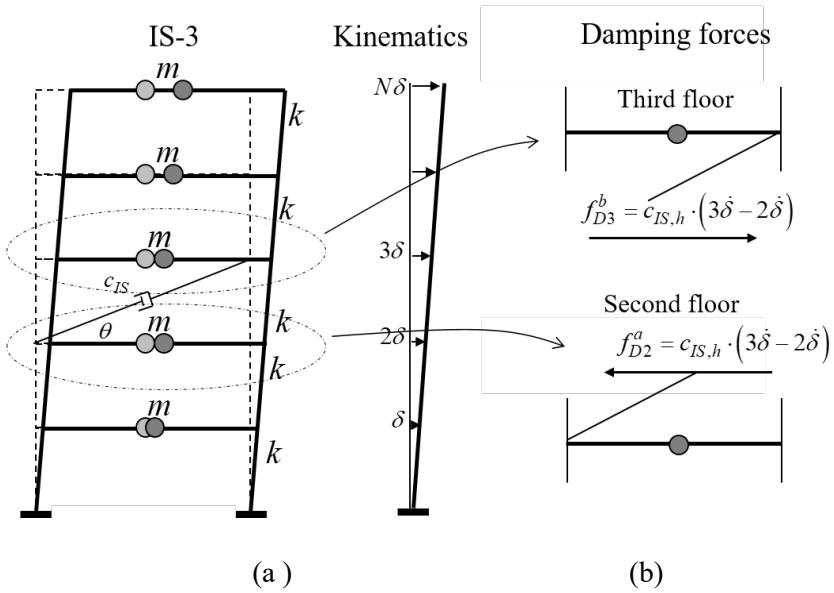

Figure 12. IS-3 system: kinematics (a) and damping forces (b).

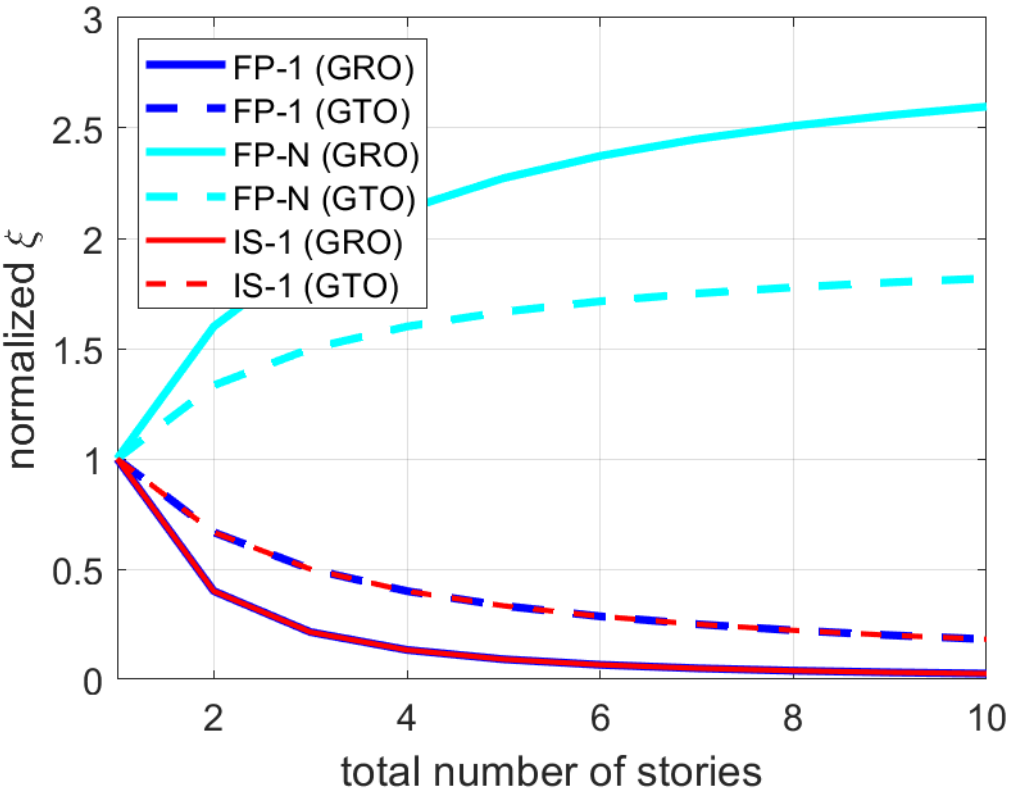

Figure 13. Normalized damping ratios vs total number of storeys for selected FP and IS systems.

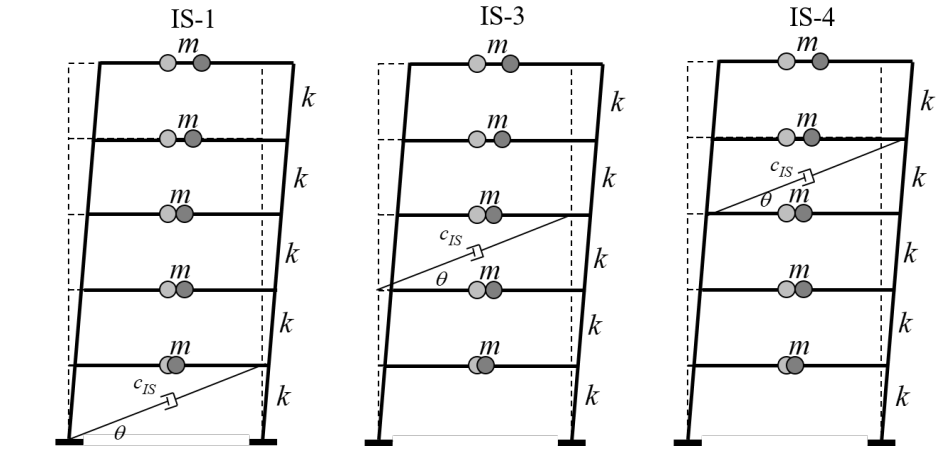

(a)

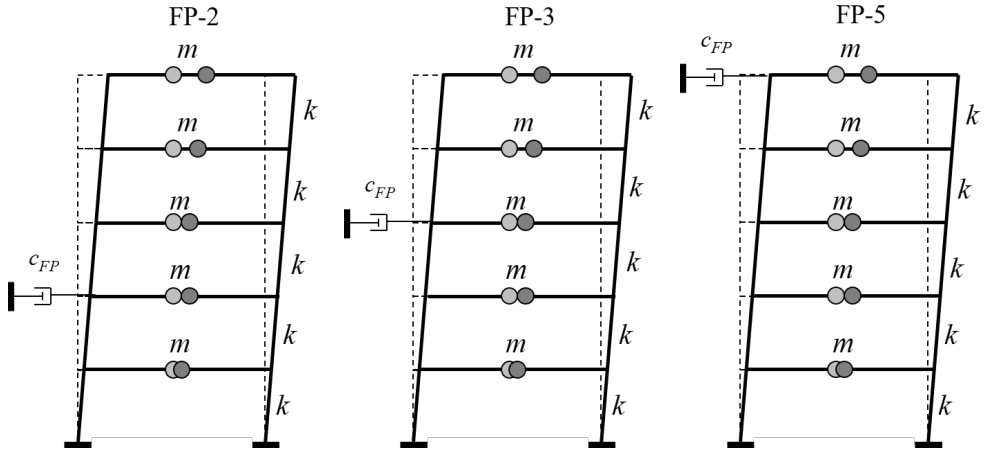

(b)

Figure 14. The analyzed systems: (a) IS systems. (b) FP systems.

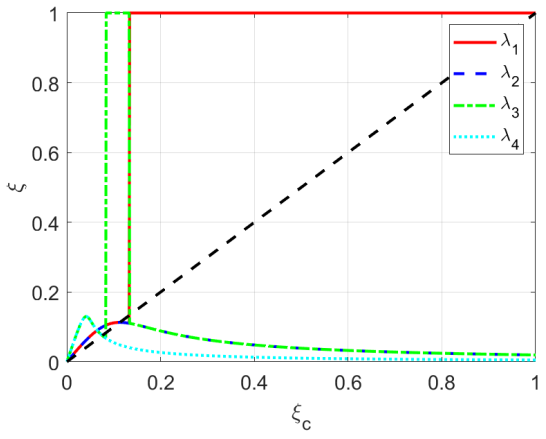

(a)

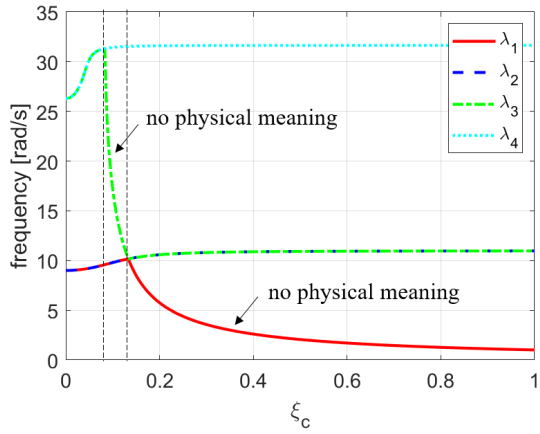

(b)

Figure 15. Systems IS-1 and FP-1: (a) damping ratios associated to first and second complex modes. (b) undamped circular frequencies associated to first and second complex modes.

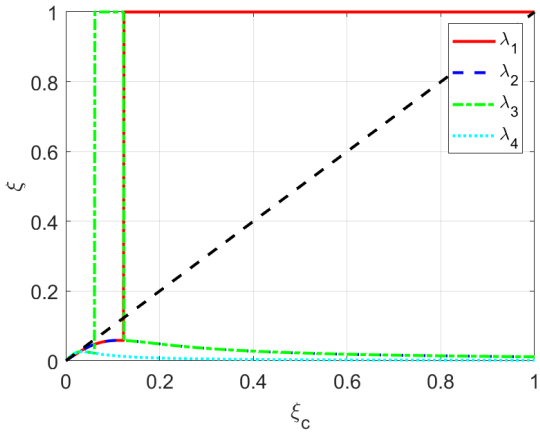

(a)

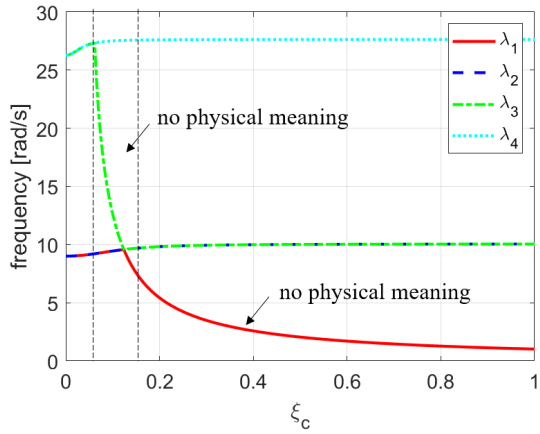

(b)

Figure 16: System IS-3: (a) damping ratios associated to first and second complex modes. (b) undamped circular frequencies associated to first and second complex modes.

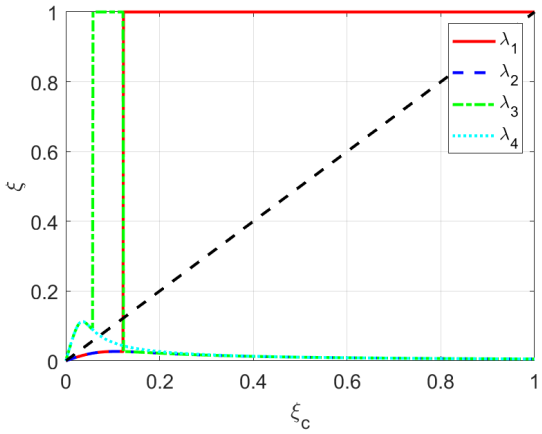

(a)

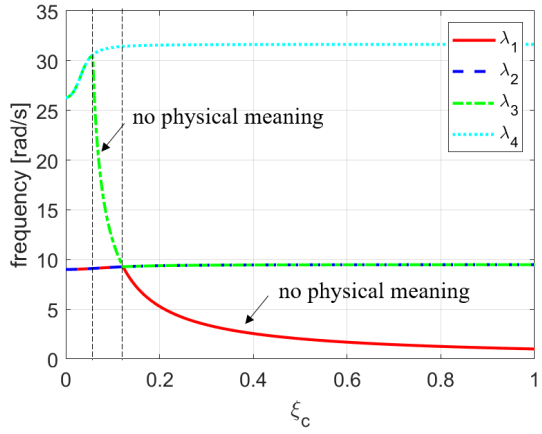

(b)

Figure 17. System IS-4: (a) damping ratios associated to first and second complex modes. (b) undamped circular frequencies associated to first and second complex modes.

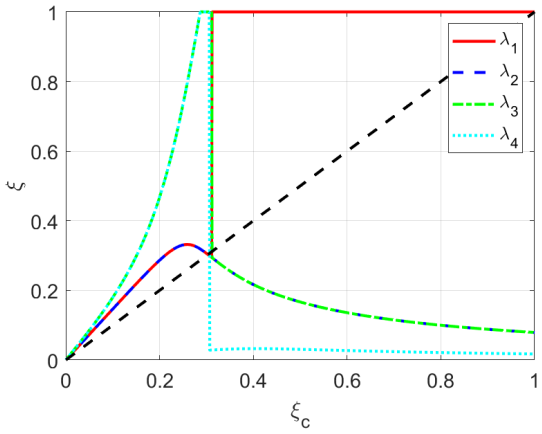

(a)

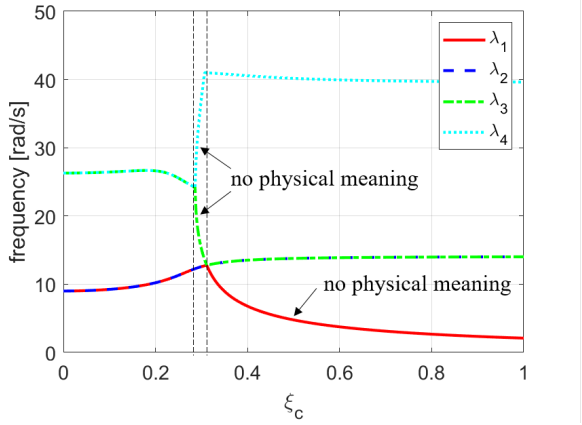

(b)

Figure 18. System FP-2: (a) damping ratios associated to first and second complex modes. (b) undamped circular frequencies associated to first and second complex modes.

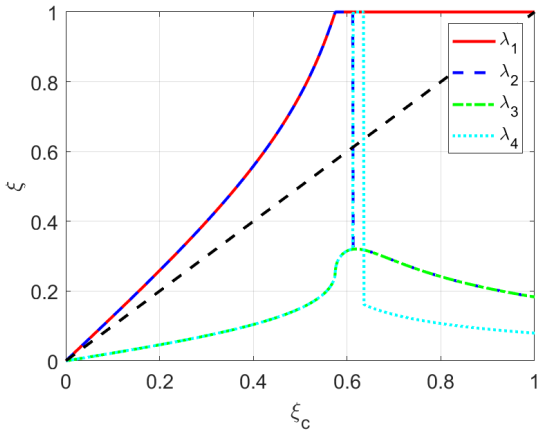

(a)

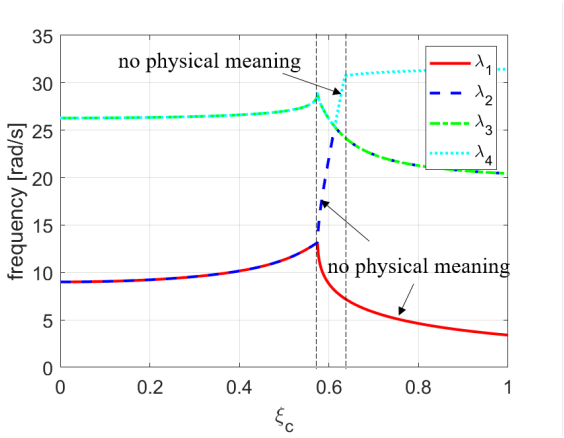

(b)

Figure 19. System FP-3: (a) damping ratios associated to first and second complex modes. (b) undamped circular frequencies associated to first and second complex modes.

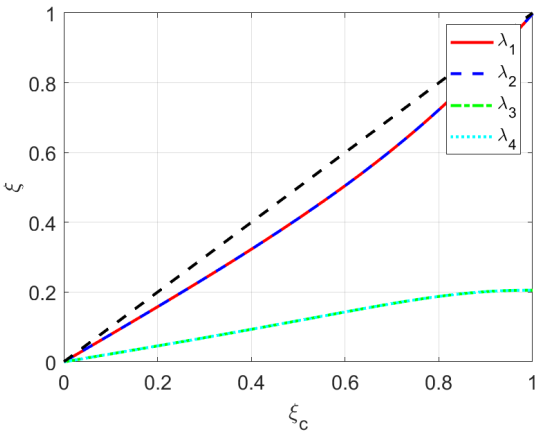

(a)

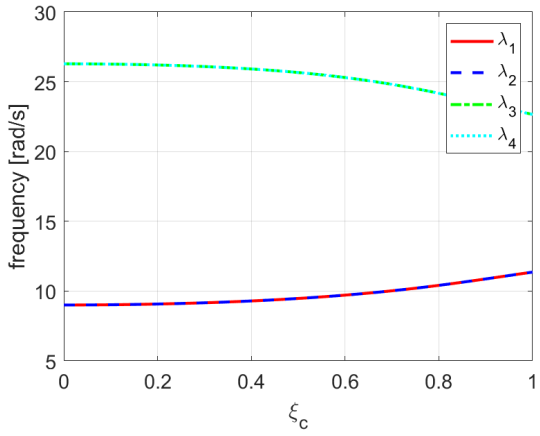

(b)

Figure 20. System FP-5: (a) damping ratios associated to first and second complex modes. (b) undamped circular frequencies associated to first and second complex modes.

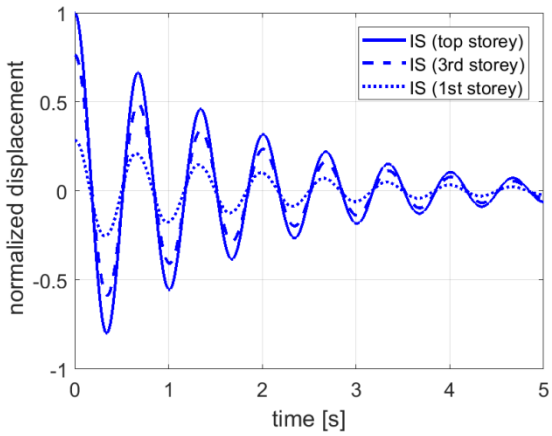

(a)

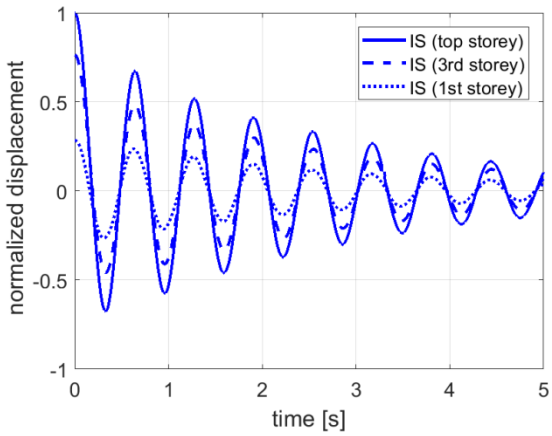

(b)

Figure 21. Time-history response under free-vibrations for system IS-2: (a) ξ_c =10%; (b) ξ_c =30%.

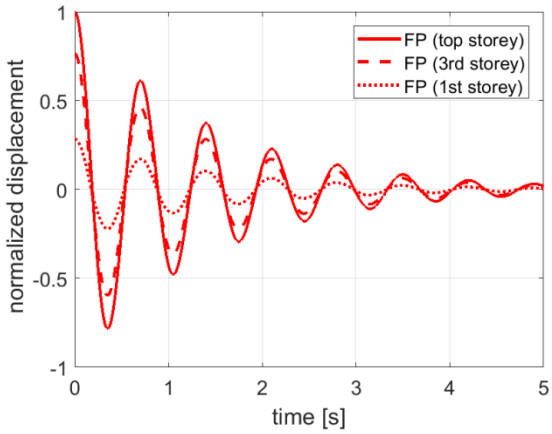

(a)

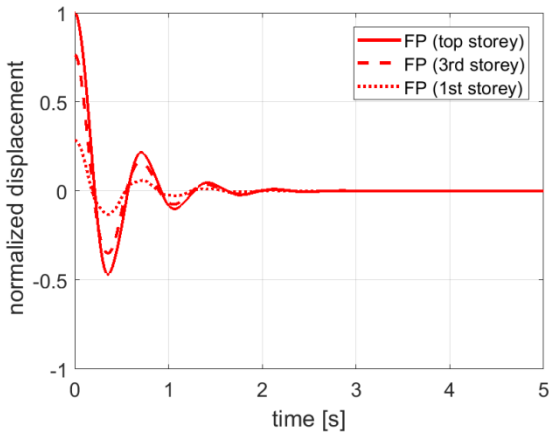

(b)

Figure 22. Time-history response under free-vibrations for system FP-5: (a) ξ_c =10%; (b) ξ_c =30%.